Published March 21, 2011

G-CSF to the *csf3r*$^{-/-}$ mice. If G-CSF functions through other receptors, the addition of G-CSF should still improve the skeletal muscle regeneration of *csf3r*$^{-/-}$ mice. Exogenous G-CSF administration didn't improve skeletal muscle regeneration (Fig. 5 f). The numbers of regenerating myocytes in the regenerating skeletal muscles were measured. G-CSF administration significantly increased the numbers of regenerating myocytes in the *csf3r*$^{+/+}$ mice but not in the *csf3r*$^{-/-}$ mice (Fig. 5 g). Functional recovery was assessed by measuring handgrip strength after cardiotoxin injection into forearm muscles.

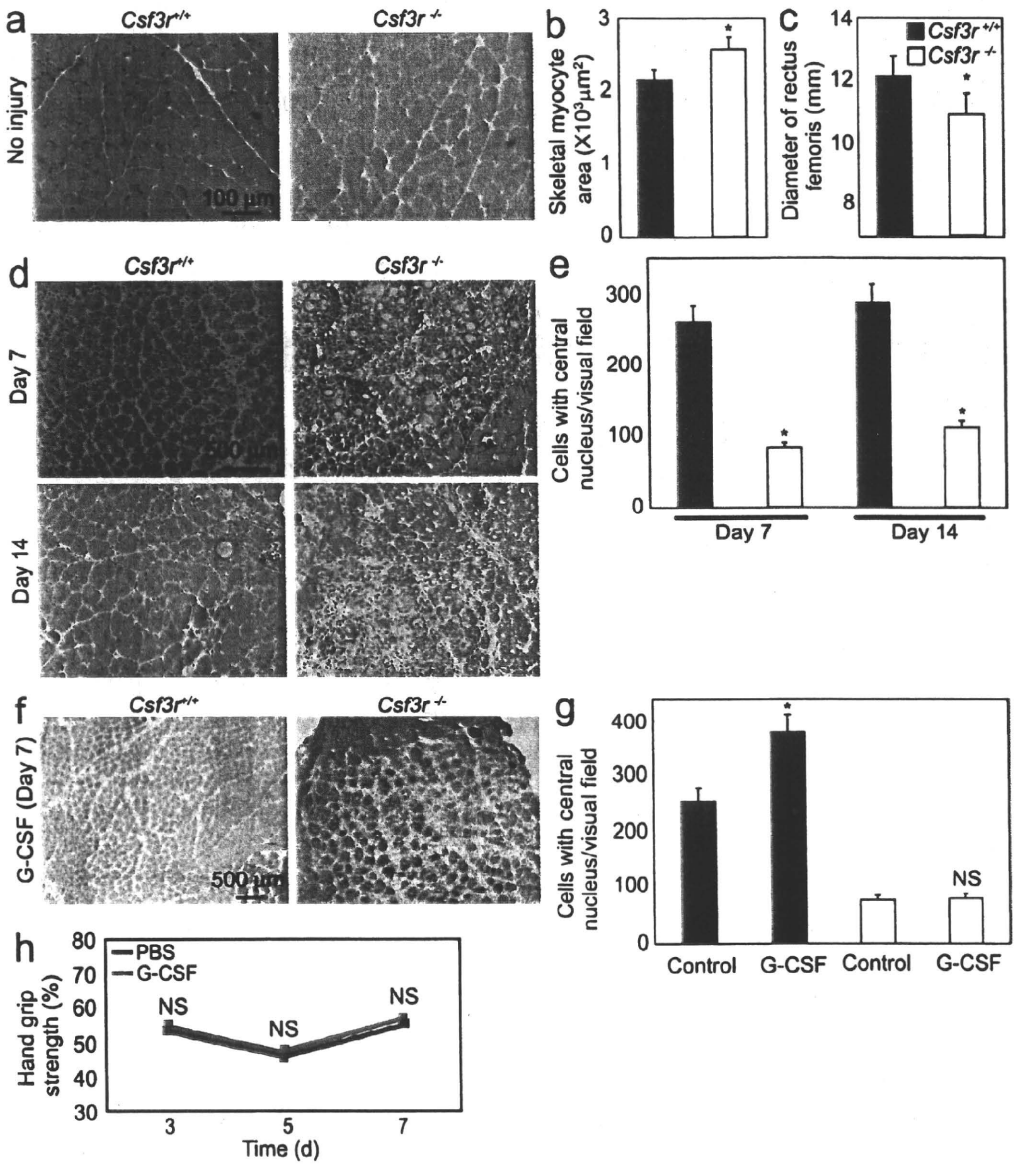

Figure 5. The *csf3r*$^{-/-}$ mouse shows impaired skeletal muscle development and regeneration. (a) Hematoxylin and eosin staining of the rectus femoris of a wild-type mouse and a *csf3r*$^{-/-}$ mouse. (b) Quantitative analysis of the areas of the skeletal myocyte sections in the wild-type and *csf3r*$^{-/-}$ mice. (c) The diameter of the rectus femoris is shown. (d) Hematoxylin and eosin staining of the cardiotoxin-injured skeletal muscles of the wild-type and *csf3r*$^{-/-}$ mice at 7 and 14 d after injury. (e) Numbers of regenerating myocytes that have centrally located nuclei on days 7 and 14 after injury in the regenerating skeletal muscles of the wild-type and *csf3r*$^{-/-}$ mice. 20 visual fields per individual mice were observed in the rectus femoris. (f) Effects of extrinsic G-CSF administration on cardiotoxin-induced muscle injury in the wild-type and *csf3r*$^{-/-}$ mice. Hematoxylin and eosin staining of injured skeletal muscle on day 7 after cardiotoxin injection is shown. (g) Effect of extrinsic G-CSF administration on cardiotoxin-induced skeletal myocyte injury, as assessed by the numbers of regenerating myocytes. 20 visual fields per individual mice were observed in the rectus femoris at 14 d after cardiotoxin injection. (b, c, e, and g) Error bars present mean ± SD (*, $P < 0.05$). (h) Handgrip strengths of cardiotoxin-injected *csf3r*$^{-/-}$ mice with or without G-CSF treatment. Results in a–h are from eight independent experiments.

Published March 21, 2011

G-CSF administration didn't confer functional recovery on day 5 or 7 after injury (Fig. 5 h). To elucidate precise myoblast function, we also examined the proliferation ability of *csf3r*$^{-/-}$ myoblasts in vitro. The *csf3r*$^{-/-}$ myoblasts showed significant decreased proliferation ability (Fig. S1 c). However, the expression of myocyte differentiation marker was not altered, which indicates that myocyte differentiation ability was not impaired in *csf3r*$^{-/-}$ myoblasts (Fig. S1 d).

G-CSFR–expressing BM cells do not recover skeletal muscle regeneration in the *csf3r*$^{-/-}$ mouse

To clarify the involvement of hematopoietic cells or BM cells in the impairment of skeletal muscle regeneration, we transplanted the BM cells from *csf3r*$^{+/+}$ mice, which constitutively expressed GFP, to the *csf3r*$^{-/-}$ mice (Fig. 6 a) 60 d before cardiotoxin-induced injury. In all the mice, the BM cells stably engrafted, and chimerism was >80%, as assessed by FACS (Fig. S3 a). After cardiotoxin injection into forearm muscles, the *csf3r*$^{-/-}$ mice that were transplanted with BM cells from *csf3r*$^{+/+}$ mice didn't show any improvement in gross morphology, the number of central cells, and handgrip strength after G-CSF treatment (Fig. 6, b–d). Moreover, the diameter of rectus femoris in these mice wasn't improved by G-CSF treatment after cardiotoxin injection into the rectus femoris muscles (Fig. 6 e). These mice showed no significant improvement in the regeneration by G-CSF treatment, and myocyte area was not altered by G-CSF treatment either (Fig. S3 b).

Next, we performed the BM transplantation experiment in reverse; the BM cells from *csf3r*$^{-/-}$ mice were transplanted into *csf3r*$^{+/+}$ mice. In these mice, skeletal muscle injury was generated, and regeneration was induced with G-CSF (Fig. 6 f). G-CSF treatment markedly improved gross morphology, the number of central cells, and handgrip strength after cardiotoxin injection into forearm muscles (Fig. 6, g–i) and increased the diameter of the rectus femoris after cardiotoxin injection into the rectus femoris muscles (Fig. 6 j). These mice showed more regeneration, and mean myocyte area was decreased by G-CSF treatment (Fig. S3 c). These results indicate that G-CSF promotion of skeletal muscle regeneration is a direct effect on skeletal muscle and isn't mediated by BM cells.

DISCUSSION

This study demonstrates that G-CSF and G-CSFR play pivotal roles in skeletal myocyte development and regeneration. Interestingly, this mechanism about G-CSF and G-CSFR is conserved between embryonic skeletal myocyte development and adult skeletal myocyte regeneration. G-CSFR is transiently but strongly expressed in myoblasts during development. The total mass of skeletal muscle is lower in *csf3r*$^{-/-}$ mice than in *csf3r*$^{+/+}$ mice, which means that G-CSF and G-CSFR signaling are essential for proper skeletal muscle development. G-CSFR is also expressed in the regenerating adult myocyte. G-CSF stimulates these G-CSFR–expressing myoblasts and promotes skeletal muscle regeneration after injury. The *csf3r*$^{-/-}$ mice showed drastic impairment of skeletal muscle regeneration, which suggests that G-CSF is critical for skeletal muscle regeneration.

During development, early muscle progenitor cells are characterized by Pax3 and Pax7 expression. Pax3 and Pax7 cooperatively specify the muscle progenitor pool because in mice deficient for both Pax3 and Pax7, all muscle progenitor cells are absent (Kassar-Duchossoy et al., 2005; Relaix et al., 2005). Once specified, muscle progenitor cells either proliferate or exit the cell cycle to undergo terminal differentiation. The latter process requires the activation of MRFs (Sabourin and Rudnicki, 2000). G-CSFR was expressed in cells that expressed MRFs but not in early muscle progenitor cells. Therefore, we speculate that rather than inducing early progenitor cells to increase the skeletal muscle stem cell pool, G-CSF causes late progenitor cells to adopt muscle mass requirement. In adult skeletal muscle, myogenic progenitor cells, which are characterized by the expression of MyoD, Myf5, or MRF4, and myoblasts, which are characterized by MyoD and Myf5 expression, are known as transient-amplifying cells (Weintraub, 1993; Shi and Garry, 2006; Kuang and Rudnicki, 2008; Biressi and Rando, 2010). We found that in the adult stage, G-CSFR was expressed in myoblasts, and G-CSF increased myocyte proliferation.

G-CSF is a hematopoietic cytokine that recruits hematopoietic cells (Cottler-Fox et al., 2003). The contribution of BM cells to muscle regeneration has been documented (Ferrari et al., 1998; Gussoni et al., 1999; LaBarge and Blau, 2002). To exclude the possibility that hematopoietic cells and BM mesenchymal stem cells affect skeletal muscle regeneration in response to G-CSF, we transferred wild-type BM cells to *csf3r*$^{-/-}$ mice. In these mice, the skeletal myocytes didn't express G-CSFR, whereas the BM cells expressed G-CSFR. If BM cells contributed to skeletal muscle regeneration, these mice would show normal or improved regeneration abilities. However, they didn't show skeletal muscle regeneration in response to G-CSF. This finding is consistent with a report that stromal progenitor cells are mobilized by vascular endothelial growth factor but not by G-CSF (Pitchford et al., 2009). We assume that the contribution of BM cells to G-CSF–mediated skeletal muscle regeneration is negligible.

Skeletal muscle regeneration is a complex process that remains to be fully understood. After muscle injury, disruption of the myofiber plasma membrane initiates an influx of extracellular calcium, leading to calcium-dependent proteolysis, which results in necrosis and degeneration of the myofibers. Several signals released from the degenerating myocytes attract and activate inflammatory cells, which secrete cytokines. Neutrophils are the first inflammatory cells to reach the injured myofibers, followed by macrophages, which phagocyte the degenerating muscle fibers (Chargé and Rudnicki, 2004). Satellite cells and macrophages interact to amplify chemotaxis and enhance inflammation. Monocytes and macrophages may support satellite cell survival by cell–cell contacts and the release of soluble factors (Chazaud et al., 2003). In addition, monocyte and macrophage infiltration leads to increased satellite cell proliferation and differentiation (Lescaudron et al., 1999).

Published March 21, 2011

Based on our results, we speculate that macrophages are not only important for the resolution of necrosis but also involved in the induction of muscle regeneration. These leukocytes secrete G-CSF in the presence of appropriate stimuli (Hareng and Hartung, 2002). Although previous studies showed that G-CSF seems to have some positive effects on skeletal muscle regeneration, it's not clear how G-CSF affects skeletal muscle regeneration, and especially the involvement

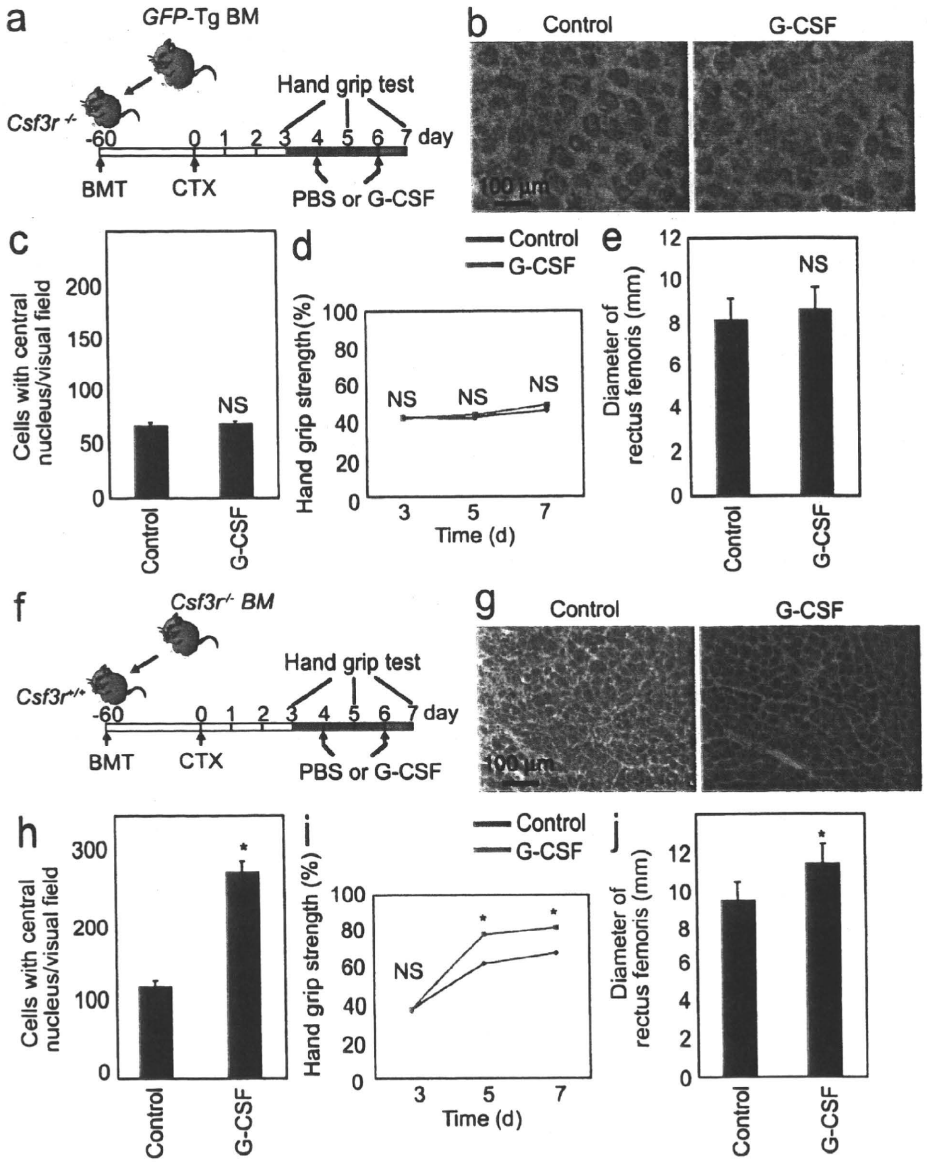

Figure 6. Effect of transplanted G-CSFR–expressing BM cells on skeletal muscle regeneration. (a) Experimental model of BM transplantation 1. BM cells were isolated from GFP-transgenic (Tg) mice and transplanted into the *csf3r*$^{-/-}$ mice. Cardiotoxin was injected into the rectus femoris, and G-CSF was administered on days 4 and 6. (b–e) Effects of G-CSF on skeletal muscle regeneration of *csf3r*$^{-/-}$ mice subjected to cardiotoxin-induced skeletal myocyte injury and transplanted with wild-type BM (from GFP-transgenic mice). (b) Hematoxylin and eosin staining of the cardiotoxin-injured skeletal muscles at 7 d after injury. (c) Effect of extrinsic G-CSF administration on cardiotoxin-induced skeletal myocyte injury, as assessed by the numbers of regenerating myocytes. 20 visual fields per individual mice were observed in the rectus femoris at 14 d after cardiotoxin injection. (d and e) Effects of G-CSF on the handgrip strength (d) and rectus femoris diameter at 14 d (e) are negligible. (f) Experimental model of BM transplantation 2. BM cells were isolated from *csf3r*$^{-/-}$ mice and transplanted into the wild-type (*csf3r*$^{+/+}$) mice. (g) Hematoxylin and eosin staining of the cardiotoxin-injured skeletal muscles at 7 d after injury. (h) Effect of extrinsic G-CSF administration on cardiotoxin-induced skeletal myocyte injury, as assessed by the numbers of regenerating myocytes. 20 visual fields per individual mice were observed in the rectus femoris at 14 d after cardiotoxin injection. (i and j) Effects of G-CSF on the handgrip strength (i) and rectus femoris diameter at 14 d (j). (c, e, and h–j) Error bars present mean ± SD (*, $P < 0.05$). Results in b–e and g–j are from eight independent experiments.

Published March 21, 2011

of G-CSFR is not well understood (Stratos et al., 2007; Naito et al., 2009). We proved that BM-derived cells were not directly involved in skeletal muscle regeneration by G-CSF; however, BM-derived cells expressing G-CSF ligand can stimulate skeletal muscle proliferation through myoblast-specific expression of G-CSFR. This study demonstrates for the first time that the factors involved in the inflammatory process switch on the process of skeletal muscle regeneration.

Clinically, G-CSF is used to treat patients with neutropenia resulting from immunosuppressive chemotherapy, severe congenital neutropenia, life-threatening infections, and stem cell harvesting (Hammond et al., 1989; Molineux et al., 1990; Welte et al., 1996). Interestingly, myalgia is one of the main side effects of G-CSF administration in humans (Taylor et al., 1989). We may speculate that innate skeletal muscle regenerates itself to some extent to adapt the physiological turn over, that G-CSF injection stimulates small population of these skeletal myoblasts, and that the burst of skeletal myocyte proliferation gives rise to myalgia. The safety and side effects of G-CSF have been studied in several clinical settings (Anderlini and Champlin, 2008). Therefore, a clinical trial of G-CSF for human skeletal muscle injury may be warranted. The results of this study underline the importance of G-CSF in skeletal muscle development and regeneration and strengthen the case for using G-CSF as a skeletal muscle regeneration therapy.

MATERIALS AND METHODS

Whole-mount in situ hybridization. Mouse embryos were removed from wild-type Institute of Cancer Research pregnant mice on E10.5. Whole-mount in situ hybridization was performed as described previously (Yuasa et al., 2005). The full-length cDNAs for mouse *c-met*, *pax3*, *myoD*, and *myf4* (available from GenBank/EMBL/DDBJ under accession numbers NM_008591, NM_001159520, NM_010866, and NM_008657 [listed as *myf6*], respectively) were provided by M.E. Buckingham (Pasteur Institute, Paris, France). The full-length cDNA for mouse *csf3r* (GenBank accession number NM_007782) was provided by S. Nagata (Osaka University, Suita, Osaka, Japan; Fukunaga et al., 1990). The probes were generated using T3 or T7 RNA polymerase.

Animals. The *myf5 nlacZ* mice were a gift from S. Tajbakhsh (Pasteur Institute; Tajbakhsh et al., 1996). The *csf3r*$^{-/-}$ mice were a gift from D.C. Link (Washington University School of Medicine, St. Louis, MO; Richards et al., 2003). All the experimental procedures and protocols were approved by the Animal Care and Use Committee of Keio University and conformed to the National Institutes of Health Guidelines for the Care and Use of Laboratory Animals.

Immunofluorescence. Mouse embryos on E8.5, E9.5, E10.5, and E11.5 were fixed in 4% paraformaldehyde for 3 h and embedded in Tissue-Tek OCT (Sakura) for frozen sectioning. The samples were incubated with Triton X-100 for 5 min at room temperature, washed, and incubated with the following primary antibodies: anti–G-CSFR (1:50; Santa Cruz Biotechnology, Inc.), anti-Pax3 (1:200; American Type Culture Collection), anti-Pax7 (1:50; R&D Systems), anti-MyoD (1:50; Dako), antimyogenin (1:50; Santa Cruz Biotechnology, Inc.), antidesmin (Dako), anti–G-CSF (1:50; Santa Cruz Biotechnology, Inc.), anti–α-actinin (1:1,000; Sigma-Aldrich), and anti-GAPDH (1:200; Santa Cruz Biotechnology, Inc.). After overnight incubation, bound antibodies were visualized with a secondary antibody conjugated to Alexa Fluor 488 or 546 (Invitrogen). Nuclei were stained with DAPI (Invitrogen). For BrdU staining, a BrdU labeling kit (Roche) was used. After antigen retrieval using HistoVT One (L6F9587; Nacalai Tesque) and blocking, BrdU staining was performed as described in the manufacturer's protocol.

Myoblast culturing. C2C12 mouse myoblasts (American Type Culture Collection) were cultured in DME/10% FBS (Invitrogen). The medium was replaced with DME/2% horse serum (Invitrogen) to induce differentiation. Recombinant mouse G-CSF (R&D Systems) was added on the indicated days. Inhibition of G-CSF signaling was analyzed by administering an anti–G-CSFR neutralizing antibody (R&D Systems).

Western blotting. C2C12 cells were treated with G-CSF. Cell extracts were prepared at 0, 5, 10, 15, 30, 45, and 60 min after G-CSF stimulation. Protein lysates were resolved by SDS-PAGE and transferred to a polyvinylidene fluoride membrane, followed by immunoblotting with anti–phospho-STAT3, anti–phospho-AKT, anti–phospho-ERK, anti–phospho-JNK, and anti–phospho-p38MAPK antibodies (all from Cell Signaling Technology) and horseradish peroxidase–conjugated anti IgG, followed by development with the SuperSignal West Pico Chemiluminescent reagent (Thermo Fisher Scientific). The same membrane was retrieved and reblotted with anti-STAT3, anti-AKT, anti-ERK, anti-JNK, and anti-p38MAPK antibodies (all from Cell Signaling Technology), respectively.

Luciferase analysis. C2C12 cells plated in DME were transfected with Lipofectamine (Invitrogen) according to the manufacturer's instructions. The APRE luciferase plasmid was provided by A. Yoshimura (Keio University, Shinjuku, Tokyo, Japan) and used at a dosage of 100 ng. The administered dosages of G-CSF were 37.5, 125.0, and 375.0 pg/ml. CMV-*Renilla* luciferase was used as an internal control to normalize for variations in transfection efficiency. All of the proteins were expressed at similar levels, as confirmed by Western blotting.

Skeletal muscle injury model. 10 μM cardiotoxin (*Naja mossambica mossambica*; Sigma-Aldrich) diluted in 100 μl PBS was injected into the rectus femoris muscles of BL6/J mice using a 27-gauge needle and a 1-ml syringe. The needle was inserted deep into the rectus femoris longitudinally to the knee. Cardiotoxin was injected along the length of the muscle. The mice in the control group were injected with 100 μl PBS. Mice (treated and control groups) were sacrificed at various time points after cardiotoxin injection, and blood samples (1.0–1.5 ml from each mouse) were collected in heparin-rinsed syringes.

Handgrip strength testing. 10 μM cardiotoxin (Sigma-Aldrich) diluted in 100 μl PBS was injected into forearm muscles of BL6/J mice. Five training sessions were performed during which the animals were held, facing the bar of the grip strength meter (Muromachi Kikai), while the forearm was gently restrained by the experimenter. When the unrestrained forepaw is brought into contact with the bar of the grip strength meter, the animal grasps the bar, after which the animal is gently pulled away from the device. The grip strength meter measures the maximal force applied before the animal released the bar.

BM transplantation. BM cells were harvested from 8-wk-old enhanced GFP (EGFP)–transgenic mice. After irradiation with a single dose of 9.0 Gy, the unfractionated EGFP$^+$ BM cells (1×10^6 cells) were injected via the tail vein, as described previously (Kawada et al., 2006). To assess chimerism, peripheral blood cells were collected from the recipient mice 60 d after BM transplantation, and the frequency of EGFP$^+$ cells in the population of peripheral nucleated blood cells was determined in a FACS sorter (BD) after hemolysis was induced with ammonium chloride to eliminate erythrocytes.

Statistical analysis. The data were analyzed using the StatView J-4.5 software (SAS Institute, Inc.). Values are reported as means ± SD. Comparisons among groups were performed by one-way analysis of variance. Scheffe's F test was used to determine the level of significance. The probability level accepted for significance was $P < 0.05$.

Published March 21, 2011

JEM

Online supplemental material. Fig. S1 shows the effect of G-CSF on myoblast differentiation in C2C12 cells and myoblasts harvested from *csf3r*$^{+/+}$ and wild-type mice. Fig. S2 shows histological analysis of cardiotoxin-injured skeletal muscle from day 1 to 28. Fig. S3 shows the chimerism of hematopoietic cells before and after BM cell transplantation and quantitative analysis of the areas of the skeletal myocyte sections in the *csf3r*$^{-/-}$ and *csf3r*$^{+/+}$ mice with BM transplantation. Online supplemental material is available at http://www.jem.org/cgi/content/full/jem.20101059/DC1.

This study was supported in part by research grants from the Ministry of Education, Culture, Sports, Science and Technology, Japan and by the Program for Promotion of Fundamental Studies in Health Science of the National Institute of Biomedical Innovation.

The authors have no conflicting financial interests.

Submitted: 26 May 2010
Accepted: 11 February 2011

REFERENCES

Aarts, L.H.J., O. Roovers, A.C. Ward, and I.P. Touw. 2004. Receptor activation and 2 distinct COOH-terminal motifs control G-CSF receptor distribution and internalization kinetics. *Blood.* 103:571–579. doi:10.1182/blood-2003-07-2250

Adams, G.R., F. Haddad, and K.M. Baldwin. 1999. Time course of changes in markers of myogenesis in overloaded rat skeletal muscles. *J. Appl. Physiol.* 87:1705–1712.

Anderlini, P., and R.E. Champlin. 2008. Biologic and molecular effects of granulocyte colony-stimulating factor in healthy individuals: recent findings and current challenges. *Blood.* 111:1767–1772. doi:10.1182/blood-2007-07-097543

Armand, A.-S., C. Pariset, I. Laziz, T. Launay, F. Fiore, B. Della Gaspera, D. Birnbaum, F. Charbonnier, and C. Chanoine. 2005. FGF6 regulates muscle differentiation through a calcineurin-dependent pathway in regenerating soleus of adult mice. *J. Cell. Physiol.* 204:297–308. doi:10.1002/jcp.20302

Avalos, B.R. 1996. Molecular analysis of the granulocyte colony-stimulating factor receptor. *Blood.* 88:761–777.

Biressi, S., and T.A. Rando. 2010. Heterogeneity in the muscle satellite cell population. *Semin. Cell Dev. Biol.* 21:845–854. doi:10.1016/j.semcdb.2010.09.003

Blau, H.M., C.-P. Chiu, and C. Webster. 1983. Cytoplasmic activation of human nuclear genes in stable heterocaryons. *Cell.* 32:1171–1180. doi:10.1016/0092-8674(83)90300-8

Bober, E., G.E. Lyons, T. Braun, G. Cossu, M. Buckingham, and H.H. Arnold. 1991. The muscle regulatory gene, Myf-6, has a biphasic pattern of expression during early mouse development. *J. Cell Biol.* 113:1255–1265. doi:10.1083/jcb.113.6.1255

Bober, E., T. Franz, H.H. Arnold, P. Gruss, and P. Tremblay. 1994. Pax-3 is required for the development of limb muscles: a possible role for the migration of dermomyotomal muscle progenitor cells. *Development.* 120:603–612.

Buckingham, M., and D. Montarras. 2008. Skeletal muscle stem cells. *Curr. Opin. Genet. Dev.* 18:330–336. doi:10.1016/j.gde.2008.06.005

Chargé, S.B.P., and M.A. Rudnicki. 2004. Cellular and molecular regulation of muscle regeneration. *Physiol. Rev.* 84:209–238. doi:10.1152/physrev.00019.2003

Chazaud, B., C. Sonnet, P. Lafuste, G. Bassez, A.-C. Rimaniol, F. Poron, F.-J. Authier, P.A. Dreyfus, and R.K. Gherardi. 2003. Satellite cells attract monocytes and use macrophages as a support to escape apoptosis and enhance muscle growth. *J. Cell Biol.* 163:1133–1143. doi:10.1083/jcb.200212046

Clever, J.L., Y. Sakai, R.A. Wang, and D.B. Schneider. 2010. Inefficient skeletal muscle repair in inhibitor of differentiation knockout mice suggests a crucial role for BMP signaling during adult muscle regeneration. *Am. J. Physiol. Cell Physiol.* 298:C1087–C1099. doi:10.1152/ajpcell.00388.2009

Cottler-Fox, M.H., T. Lapidot, I. Petit, O. Kollet, J.F. DiPersio, D. Link, and S. Devine. 2003. Stem cell mobilization. *Hematology (Am. Soc. Hematol. Educ. Program).* 419–437.

Demetri, G.D., and J.D. Griffin. 1991. Granulocyte colony-stimulating factor and its receptor. *Blood.* 78:2791–2808.

Ferrari, G., G. Cusella-De Angelis, M. Coletta, E. Paolucci, A. Stornaiuolo, G. Cossu, and F. Mavilio. 1998. Muscle regeneration by bone marrow-derived myogenic progenitors. *Science.* 279:1528–1530. doi:10.1126/science.279.5356.1528

Fukunaga, R., Y. Seto, S. Mizushima, and S. Nagata. 1990. Three different mRNAs encoding human granulocyte colony-stimulating factor receptor. *Proc. Natl. Acad. Sci. USA.* 87:8702–8706. doi:10.1073/pnas.87.22.8702

Gussoni, E., Y. Soneoka, C.D. Strickland, E.A. Buzney, M.K. Khan, A.F. Flint, L.M. Kunkel, and R.C. Mulligan. 1999. Dystrophin expression in the mdx mouse restored by stem cell transplantation. *Nature.* 401:390–394.

Hammond, W.P. IV, T.H. Price, L.M. Souza, and D.C. Dale. 1989. Treatment of cyclic neutropenia with granulocyte colony-stimulating factor. *N. Engl. J. Med.* 320:1306–1311. doi:10.1056/NEJM198905183202003

Harada, M., Y. Qin, H. Takano, T. Minamino, Y. Zou, H. Toko, M. Ohtsuka, K. Matsuura, M. Sano, J. Nishi, et al. 2005. G-CSF prevents cardiac remodeling after myocardial infarction by activating the Jak-Stat pathway in cardiomyocytes. *Nat. Med.* 11:305–311. doi:10.1038/nm1199

Hareng, L., and T. Hartung. 2002. Induction and regulation of endogenous granulocyte colony-stimulating factor formation. *Biol. Chem.* 383:1501–1517. doi:10.1515/BC.2002.172

Hosaka, Y., T. Yokota, Y. Miyagoe-Suzuki, K. Yuasa, M. Imamura, R. Matsuda, T. Ikemoto, S. Kameya, and S.i. Takeda. 2002. α1-syntrophin–deficient skeletal muscle exhibits hypertrophy and aberrant formation of neuromuscular junctions during regeneration. *J. Cell Biol.* 158:1097–1107. doi:10.1083/jcb.200204076

Jostes, B., C. Walther, and P. Gruss. 1990. The murine paired box gene, Pax7, is expressed specifically during the development of the nervous and muscular system. *Mech. Dev.* 33:27–37. doi:10.1016/0925-4773(90)90132-6

Kassar-Duchossoy, L., E. Giacone, B. Gayraud-Morel, A. Jory, D. Gomès, and S. Tajbakhsh. 2005. Pax3/Pax7 mark a novel population of primitive myogenic cells during development. *Genes Dev.* 19:1426–1431. doi:10.1101/gad.345505

Kawada, H., S. Takizawa, T. Takanashi, Y. Morita, J. Fujita, K. Fukuda, S. Takagi, H. Okano, K. Ando, and T. Hotta. 2006. Administration of hematopoietic cytokines in the subacute phase after cerebral infarction is effective for functional recovery facilitating proliferation of intrinsic neural stem/progenitor cells and transition of bone marrow-derived neuronal cells. *Circulation.* 113:701–710. doi:10.1161/CIRCULATIONAHA.105.563668

Kuang, S., and M.A. Rudnicki. 2008. The emerging biology of satellite cells and their therapeutic potential. *Trends Mol. Med.* 14:82–91. doi:10.1016/j.molmed.2007.12.004

LaBarge, M.A., and H.M. Blau. 2002. Biological progression from adult bone marrow to mononucleate muscle stem cell to multinucleate muscle fiber in response to injury. *Cell.* 111:589–601. doi:10.1016/S0092-8674(02)01078-4

Le Grand, F., and M.A. Rudnicki. 2007. Skeletal muscle satellite cells and adult myogenesis. *Curr. Opin. Cell Biol.* 19:628–633. doi:10.1016/j.ceb.2007.09.012

Lescaudron, L., E. Peltékian, J. Fontaine-Pérus, D. Paulin, M. Zampieri, L. Garcia, and E. Parrish. 1999. Blood borne macrophages are essential for the triggering of muscle regeneration following muscle transplant. *Neuromuscul. Disord.* 9:72–80. doi:10.1016/S0960-8966(98)00111-4

Megeney, L.A., R.L.S. Perry, J.E. LeCouter, and M.A. Rudnicki. 1996. bFGF and LIF signaling activates STAT3 in proliferating myoblasts. *Dev. Genet.* 19:139–145. doi:10.1002/(SICI)1520-6408(1996)19:2<139::AID-DVG5>3.0.CO;2-A

Messina, G., and G. Cossu. 2009. The origin of embryonic and fetal myoblasts: a role of Pax3 and Pax7. *Genes Dev.* 23:902–905. doi:10.1101/gad.1797009

Metcalf, D. 2008. Hematopoietic cytokines. *Blood.* 111:485–491. doi:10.1182/blood-2007-03-079681

Molineux, G., Z. Pojda, I.N. Hampson, B.I. Lord, and T.M. Dexter. 1990. Transplantation potential of peripheral blood stem cells induced by granulocyte colony-stimulating factor. *Blood.* 76:2153–2158.

Naito, T., K. Goto, S. Morioka, Y. Matsuba, T. Akema, T. Sugiura, Y. Ohira, M. Beppu, and T. Yoshioka. 2009. Administration of granulocyte colony-stimulating factor facilitates the regenerative process of injured mice skeletal muscle via the activation of Akt/GSK3alphabeta signals. *Eur. J. Appl. Physiol.* 105:643–651. doi:10.1007/s00421-008-0946-9

Philippou, A., A. Halapas, M. Maridaki, and M. Koutsilieris. 2007. Type I insulin-like growth factor receptor signaling in skeletal muscle regeneration and hypertrophy. *J. Musculoskelet. Neuronal Interact.* 7:208–218.

Pitchford, S.C., R.C. Furze, C.P. Jones, A.M. Wengner, and S.M. Rankin. 2009. Differential mobilization of subsets of progenitor cells from the bone marrow. *Cell Stem Cell.* 4:62–72. doi:10.1016/j.stem.2008.10.017

Rantanen, J., T. Hurme, R. Lukka, J. Heino, and H. Kalimo. 1995. Satellite cell proliferation and the expression of myogenin and desmin in regenerating skeletal muscle: evidence for two different populations of satellite cells. *Lab. Invest.* 72:341–347.

Relaix, F., D. Rocancourt, A. Mansouri, and M. Buckingham. 2005. A Pax3/Pax7-dependent population of skeletal muscle progenitor cells. *Nature.* 435:948–953. doi:10.1038/nature03594

Rhodes, S.J., and S.F. Konieczny. 1989. Identification of MRF4: a new member of the muscle regulatory factor gene family. *Genes Dev.* 3:2050–2061. doi:10.1101/gad.3.12b.2050

Richards, M.K., F. Liu, H. Iwasaki, K. Akashi, and D.C. Link. 2003. Pivotal role of granulocyte colony-stimulating factor in the development of progenitors in the common myeloid pathway. *Blood.* 102:3562–3568. doi:10.1182/blood-2003-02-0593

Sabourin, L.A., and M.A. Rudnicki. 2000. The molecular regulation of myogenesis. *Clin. Genet.* 57:16–25. doi:10.1034/j.1399-0004.2000.570103.x

Sakuma, K., K. Watanabe, M. Sano, I. Uramoto, and T. Totsuka. 2000. Differential adaptation of growth and differentiation factor 8/myostatin, fibroblast growth factor 6 and leukemia inhibitory factor in overloaded, regenerating and denervated rat muscles. *Biochim. Biophys. Acta.* 1497:77–88. doi:10.1016/S0167-4889(00)00044-6

Serrano, A.L., B. Baeza-Raja, E. Perdiguero, M. Jardí, and P. Muñoz-Cánoves. 2008. Interleukin-6 is an essential regulator of satellite cell-mediated skeletal muscle hypertrophy. *Cell Metab.* 7:33–44. doi:10.1016/j.cmet.2007.11.011

Shi, X., and D.J. Garry. 2006. Muscle stem cells in development, regeneration, and disease. *Genes Dev.* 20:1692–1708. doi:10.1101/gad.1419406

Shimoji, K., S. Yuasa, T. Onizuka, F. Hattori, T. Tanaka, M. Hara, Y. Ohno, H. Chen, T. Egasgira, T. Seki, et al. 2010. G-CSF promotes the proliferation of developing cardiomyocytes in vivo and in derivation from ESCs and iPSCs. *Cell Stem Cell.* 6:227–237. doi:10.1016/j.stem.2010.01.002

Solomon, A.M., and P.M.G. Bouloux. 2006. Modifying muscle mass - the endocrine perspective. *J. Endocrinol.* 191:349–360. doi:10.1677/joe.1.06837

Stratos, I., R. Rotter, C. Eipel, T. Mittlmeier, and B. Vollmar. 2007. Granulocyte-colony stimulating factor enhances muscle proliferation and strength following skeletal muscle injury in rats. *J. Appl. Physiol.* 103:1857–1863. doi:10.1152/japplphysiol.00066.2007

Tajbakhsh, S., D. Rocancourt, and M. Buckingham. 1996. Muscle progenitor cells failing to respond to positional cues adopt non-myogenic fates in myf-5 null mice. *Nature.* 384:266–270. doi:10.1038/384266a0

Tapscott, S.J., R.L. Davis, M.J. Thayer, P.F. Cheng, H. Weintraub, and A.B. Lassar. 1988. MyoD1: a nuclear phosphoprotein requiring a Myc homology region to convert fibroblasts to myoblasts. *Science.* 242:405–411. doi:10.1126/science.3175662

Taylor, K.M., S. Jagannath, G. Spitzer, J.A. Spinolo, S.L. Tucker, B. Fogel, F.F. Cabanillas, F.B. Hagemeister, and L.M. Souza. 1989. Recombinant human granulocyte colony-stimulating factor hastens granulocyte recovery after high-dose chemotherapy and autologous bone marrow transplantation in Hodgkin's disease. *J. Clin. Oncol.* 7:1791–1799.

Venters, S.J., S. Thorsteinsdóttir, and M.J. Duxson. 1999. Early development of the myotome in the mouse. *Dev. Dyn.* 216:219–232. doi:10.1002/(SICI)1097-0177(199911)216:3<219::AID-DVDY1>3.0.CO;2-J

Weintraub, H. 1993. The MyoD family and myogenesis: redundancy, networks, and thresholds. *Cell.* 75:1241–1244. doi:10.1016/0092-8674(93)90610-3

Welte, K., J. Gabrilove, M.H. Bronchud, E. Platzer, and G. Morstyn. 1996. Filgrastim (r-metHuG-CSF): the first 10 years. *Blood.* 88:1907–1929.

Yan, Z., S. Choi, X. Liu, M. Zhang, J.J. Schageman, S.Y. Lee, R. Hart, L. Lin, F.A. Thurmond, and R.S. Williams. 2003. Highly coordinated gene regulation in mouse skeletal muscle regeneration. *J. Biol. Chem.* 278:8826–8836. doi:10.1074/jbc.M209879200

Yang, X.M., K. Vogan, P. Gros, and M. Park. 1996. Expression of the met receptor tyrosine kinase in muscle progenitor cells in somites and limbs is absent in Splotch mice. *Development.* 122:2163–2171.

Yuasa, S., Y. Itabashi, U. Koshimizu, T. Tanaka, K. Sugimura, M. Kinoshita, F. Hattori, S. Fukami, T. Shimazaki, S. Ogawa, et al. 2005. Transient inhibition of BMP signaling by Noggin induces cardiomyocyte differentiation of mouse embryonic stem cells. *Nat. Biotechnol.* 23:607–611. doi:10.1038/nbt1093

Yuasa, S., T. Onizuka, K. Shimoji, Y. Ohno, T. Kageyama, S.H. Yoon, T. Egashira, T. Seki, H. Hashimoto, T. Nishiyama, et al. 2010. Zac1 is an essential transcription factor for cardiac morphogenesis. *Circ. Res.* 106:1083–1091. doi:10.1161/CIRCRESAHA.109.214130

Zaruba, M.M., H.D. Theiss, M. Vallaster, U. Mehl, S. Brunner, R. David, R. Fischer, L. Krieg, E. Hirsch, B. Huber, et al. 2009. Synergy between CD26/DPP-IV inhibition and G-CSF improves cardiac function after acute myocardial infarction. *Cell Stem Cell.* 4:313–323. doi:10.1016/j.stem.2009.02.013

温泉科学（J. Hot Spring Sci.），60，375-379（2010）

日本温泉科学会第63回大会

公開講演II「温泉の価値を識る―健康と美容」1

水素水の抗酸化作用：水素水は身体にいいか？

太田成男[1)]

Anti-Oxidation Effect of Hydrogen Water : Is It Effective for Our Health?

Shigeo OHTA[1)]

1. 水素水とは何か？

一般に，砂糖を水に溶かした溶液を「砂糖水」といい，食塩を水に溶かした溶液を「食塩水」という．そして，水素分子（H_2）を水に溶かした溶液を「水素水」と呼ぶ．水素分子が水に溶けている状態は，酸素分子（O_2）が水に溶けている状態とほぼ同じと考えればよい．酸素分子が水に溶けることは，魚が水の中の酸素分子を取り入れて呼吸していることからよくわかる．

水素分子は，1気圧の水素ガスと水が接していれば常温で0.8 mM程度溶ける．重量濃度でいうと1.6 ppm（parts per million）である．溶存水素分子量をppm表示するとその値は小さいので，水素分子は溶けにくいような印象を与えるかもしれないが，分子量が小さいので重量濃度では値が小さくなるだけである．また，水素分子の溶解度は温度によって，あまり変動せず100℃でも0.4 mM溶ける．水素水には暖めて飲むこともできる利点がある．

水素分子は，プラスチックを透過するので，保存するにはアルミニウム（あるいは酸化アルミニウム）の容器を必要とする．したがって，ペットボトルで販売されている水があったら，それは水素水ではないと判断してよい．

2. 水素分子の効果

砂糖水が甘いのは，砂糖が溶けたために水自身が甘くなったのではなく，砂糖が甘いのである．水分子の性質が変化したわけではない．水素水（すなわち水素分子が溶けた水）に何らかの効果があるとすれば，水の物理的性質が変化した訳ではなく，水素分子自身に何らかの効果があるはずである．

[1)] 日本医科大学大学院医学研究科加齢科学系専攻　〒211-8533　川崎市中原区小杉町1-396. [1)] Institute of Development and Ageing Sciences, Graduate School of Medicine, Nippon Medical School, 1-396 Kosugi-machi, Nakahara-ku, Kawasaki 211-8533, Japan.

そこで筆者らは，水素分子の抗酸化効果を以下の順により調べた．

1)　無細胞化学反応系における水素分子の反応性

試験管内で，スーパーオキシド（$\cdot O_2^-$），過酸化水素（H_2O_2），ヒドロキシルラジカル（$\cdot OH$），過酸化亜硝酸（$ONOO^-$），一酸化窒素（NO）をそれぞれ化学反応によって発生させ，溶液にとけた水素分子によって還元できるかどうかを調べた．すると，酸化力の強いヒドロキシルラジカルと過酸化亜硝酸を水素分子は還元し，その他の活性酸素種は還元しないことがわかった．

2)　培養細胞による水素分子の効果

培養液に水素分子を溶かして，培養細胞中で水素分子が活性酸素種を還元できるかどうかを調べた．ヒドロキシルラジカルの半定量は蛍光色素の蛍光強度，電子スピン共鳴にて測定した．無細胞実験系と同じように水素分子はヒドロキシルラジカルを選択的に還元し，実際に細胞障害性を軽減することを明らかにした．

3)　水素ガスの吸引効果．再還流

水素ガスを吸引させることによって脳，心臓（ラット），肝臓（マウス）の虚血再灌流障害が軽減された．新生仔の低酸素による脳細胞死を水素ガス吸引が抑制した（ラット）．小腸移植が水素ガスを吸引させることによって改善された（ラット）．これらの結果で強調したいのは，(a) 水素ガス濃度は2%程度で十分効果を発揮したこと，(b) 認可されている他の医薬品よりも効果的であったことである．

3.　水素分子の安全性

「水素は身体にいいか？」を論じる前に，まず安全性について述べたい．

1)　水素分子は爆発するか？

水素というと爆発のイメージを持たれる方が多いようだが，水素分子は空気中でも4.7%以下の濃度なら，火を近づけても燃えないし，爆発もしない．水素ガスボンベを病室に持ち込んでも法的には問題はない．1937年の飛行船ヒンデンブルグ号での爆発は有名であるが，記録映画でみると白黒画像でも炎が見える．水素分子が燃えるときには炎は見えない．実は，ヒンデンブルグ号の爆発でも，水素分子が最初に燃えたのではないことは明らかである．

2)　水素水を飲んでも酸欠にはならない．

水素分子は，通常の温度ではプラチナ金属や銅金属のような触媒なしには，酸素と反応して水になることはない．したがって，水素分子を体内に取り入れても，酸欠（酸素不足）になることはない．

触媒学会のホームページ（http : //www.shokubai.org/general/kaisetsu/genri.html）で「触媒とは？」のページでは「水素と酸素から水が生成する反応 $H_2 + 1/2\ O_2 \rightarrow H_2O$ を考えてみましょう．水素と酸素の混合ガスをガラス容器に入れ200℃に加熱しても何の反応も起こりません．」と記載されている．

3)　食品としての安全性が認められている．

水素分子は既存添加物の番号192として食品として使う事が厚生労働省から認められている．既

存添加物とは，1995 年の食品衛生法及び栄養改善法の一部を改正する法律附則第 2 条第 4 項で規定される既存添加物名簿に収録された食品添加物のことで，1996 年，既存添加物名簿の告示が行われた．既存添加物の安全性評価に関する調査研究は，平成 8 年，11 年，15 年，16 年，19 年と 5 回にわたり続けられ，安全性に問題があると認められた物質は名簿から順次削除されている．したがって，水素分子は，度重なる安全性の調査研究によって，安全性が認められていると言える．また，催奇性も認められない．

4）副作用について

効果があれば副作用もあるというのが一般的な考え方である．しかし，副作用が無視できない薬剤もあれば，副作用が軽度のものもある．副作用が顕著になる理由として，過剰摂取，体内の蓄積，体内における有害物質への変化などがあげられる．しかし，水素分子の副作用はほとんどないと予想される．まず，水を飲める限界があるので，水素水として摂取する場合には水素分子の過剰摂取はありえない．錠剤のサプリメントなら茶碗いっぱいに食べることも可能だが，水素水では 10 L の水素水を飲むことはまず不可能である．また，余分な水素分子は水素ガスとして体外へ放出されてしまうので，体内に蓄積することはない．水素分子は，ヒドロキシルラジカルと反応した後は水分子となるので，有害物質には変化しない．

5）必要な活性酸素種を還元しない．

近年，抗酸化サプリメントの過剰摂取による弊害が多数報告されている．工業的に合成したある種の抗酸化サプリメントを摂取した人はむしろ短命であることが疫学調査から判明した．スーパーオキシド，過酸化水素や一酸化窒素は体内のシグナルとして重要な役割をはたしている必要な活性酸素種をも還元してしまうために，害の消去よりも益の消去が勝ってしまったためだろう．前述のように，水素分子は，これらの必要な活性酸素種を還元しないので，従来の抗酸化物質より生じる弊害は，遥かに少ないと予想できる．

6）潜水病の予防としての水素ガスの利用

深水においては高圧のために窒素ガスが血液に過剰に溶ける．急激に減圧させると窒素の気泡が生じ潜水病になる．窒素ガスの気泡が抹消血管を塞いでしまうためである．窒素ガスの代わりに，水素ガスあるいはヘリウムとの混合ガスを吸うことによって，潜水病を予防することができることが広く知られている．この方法は実際に使われており，水素ガスを長期にわたって吸い続けても何ら副作用が生じないことが証明されている．高圧下では，窒素分子（N_2）は麻酔作用を示すが，水素分子は麻酔作用もない．水素分子は，むしろ窒素分子よりも安全であると言える．

4.　水素水の顕著な飲用効果

1）短期投与の効果

短期投与として，抗がん剤のシスプラチンの副作用の軽減作用についてマウスで調べた．シスプラチンは腎臓に蓄積し，酸化ストレスを上昇させ，腎障害をおこす．水素水を自由摂取されると，形態学的にも機能的にも腎障害は軽減し，致死率も低下した．

2）身体的拘束による認知機能低下を抑制

拘束することで長期間身体的ストレスを与えたマウスは，学習・記憶能力の認知機能が低下す

る．このマウスに6週間水素水を与えるとその低下を予防することができた．拘束により脳における酸化ストレスの蓄積と歯状回神経前駆細胞の増殖低下が観察されるが，そのいずれも水素水によって抑制された．

3)　長期投与

動脈硬化の原因として，LDL-コレステロールの酸化があげられる．そこで，動脈硬化が促進されるマウスとして，apoEノックアウトマウスに水素水を自由に飲ませた．厳密に比較したわけではないが，同じapoEノックアウトマウスを用いた実験結果と比較すると，葉酸，ビタミンE，α-リポ酸よりも水素水がより効果的であった．

4)　その他

水素水の共通な効果は，抗酸化作用である．さらに，水素水を利用して動物実験を始めた研究者にとって，予想していたよりもはるかに効果が顕著であった，ということが共通の感想である．厳密な比較実験が必要であるが，現段階では，他の抗酸化物質よりも非常に効果的であると言える．さらに，当初予想していたよりも低濃度の水素濃度でも効果が見られた．飽和5%の水素水を飲ませただけで，パーキンソン病モデルマウスの予防効果を示すことが報告され，私の研究室でも飽和10%の水素水の飲用による効果をマウスで認めている．今後，厳密に同じ条件で他の抗酸化物質と比較して，水素分子の優位性を明らかにするのが課題のひとつである．

その抗酸化作用効果に加えて，抗炎症作用と抗アレルギー作用が認められるようになった．これらの複合的な作用が相乗効果を発揮して，水素分子の顕著な効果を示すのかもしれない．そして，水素分子には，生体内シグナルとして機能している可能性が浮上してきた．水素分子の効果がどの程度まで多彩な機能を有するのかを明確にしていくことと，そのメカニズムを解明することが，今後の課題である．

5.　水素医学の広がり

さらに，水素分子を溶かした生理的食塩水（水素生食）を，静脈注射や，腹腔への注射した効果も多数報告された．水素水を飲む効果は，健康維持や予防医学に適しているように思われるが，水素生食の注射は緊急時の治療に効果的であるように思われる．

また，水素生食を点眼することによって，眼の治療に効果があることも示唆された．水素生食を点眼するだけで，眼球の中にまで到達できる事を示したので，水素分子は体内の隅々まで拡散で行き渡ることが実際に示された．

6.　臨床試験

動物実験を基盤にして，実際に人に対しての水素水の臨床試験が始まっている．すでに，臨床試験の報告は3報に及び，現在，少なからず数の臨床試験が進行している．

二型糖尿病患者30名に対し，無作為割付二重盲験で一日900 mLの水素水を8週間飲ませた．その結果，2種類の酸化ストレスマーカーの減少を認めた．他のマーカーが変動しなかったので，水素分子の副作用は認められなかった．境界型糖尿病6人患者では糖負荷試験の結果が改善した．

7. 蛇足的な注意書き

現段階では，水素水の効果は動物実験で確認され，様々な疾患への予防効果が期待されている．しかし，医薬品として認可されているわけではなく，薬事法でいう「効果効能」を明記できる段階にも達していない．現段階では，水素水は安全な飲料水として販売されている．

なお，本稿では，水素分子，水素ガス，水素水という表記をし，わざわざ水素分子と分子をつけて記載したのは，水素という名のつく非科学的な商品がいろいろ販売されているからである．活性水素（原子状水素＝H）やマイナス水素イオン（H^-）のような体内で存在し得ない物質を標榜する商品は，本稿とは無関係である．水素は通常の状態では H_2 という分子あるいは H^+ というプラスイオン（陽イオン）で存在する．

文　献

関連文献は，ホームページに逐次掲載しているので参照していただきたい．
http : //hra-japan.org/paper.htm

Available online at www.sciencedirect.com
ScienceDirect
Journal of Nutritional Biochemistry 21 (2010) 381–389
Journal of Nutritional Biochemistry

Astaxanthin protects mitochondrial redox state and functional integrity against oxidative stress

Alexander M. Wolf[a], Sadamitsu Asoh[a], Hidenori Hiranuma[a], Ikuroh Ohsawa[a,b], Kumiko Iio[c], Akira Satou[c], Masaharu Ishikura[c], Shigeo Ohta[a,*]

[a]Department of Biochemistry and Cell Biology, Institute of Development and Aging Sciences, Nippon Medical School, Nakahara-ku, Kawasaki, Kanagawa 211-8533, Japan
[b]The Center of Molecular Hydrogen Medicine, Institute of Development and Aging Sciences, Nippon Medical School, 1-396 Kosugi-cho, Nakahara-ku, Kawasaki, Kanagawa 211-8533, Japan
[c]Life Science Institute, Yamaha Motor Co. Ltd., 3001-10 Kuno, Fukuroi, Shizuoka 437-0061, Japan

Received 6 August 2008; received in revised form 8 January 2009; accepted 12 January 2009

Abstract

Mitochondria combine the production of energy with an efficient chain of reduction–oxidation (redox) reactions but also with the unavoidable production of reactive oxygen species. Oxidative stress leading to mitochondrial dysfunction is a critical factor in many diseases, such as cancer and neurodegenerative and lifestyle-related diseases. Effective antioxidants thus offer great therapeutic and preventive promise. Investigating the efficacy of antioxidants, we found that a carotenoid, astaxanthin (AX), decreased physiologically occurring oxidative stress and protected cultured cells against strong oxidative stress induced with a respiratory inhibitor. Moreover, AX improved maintenance of a high mitochondrial membrane potential and stimulated respiration. Investigating how AX stimulates and interacts with mitochondria, a redox-sensitive fluorescent protein (roGFP1) was stably expressed in the cytosol and mitochondrial matrix to measure the redox state in the respective compartments. AX at nanomolar concentrations was effective in maintaining mitochondria in a reduced state. Additionally, AX improved the ability of mitochondria to remain in a reduced state under oxidative challenge. Taken together, these results suggest that AX is effective in improving mitochondrial function through retaining mitochondria in the reduced state.

Keywords: Oxidative stress; Mitochondrial membrane potential; Oxygen consumption; Redox-sensitive GFP; Astaxanthin; Metabolic syndrome

1. Introduction

Oxidative stress is involved in the pathogenesis of atherosclerosis [1,2], cancer [3], diabetes [4,5], neurodegenerative [6–8] and other diseases, as well as in the aging process itself. Antioxidant treatment has therefore great promise in alleviating some of the detrimental effects of oxidative stress [9], and several types of antioxidants stimulate lipid oxidation, which may have merit in improving metabolic syndrome [10–12]. A huge selection of both natural and synthetic antioxidants is available and can be ingested easily with, in the case of food-derived antioxidants, little concern about adverse side effects. This attractiveness has on one hand led a multi-billion dollar supplement industry often based on anecdotal evidence [13,14] and, on the other hand, to large-scale clinical trials to determine efficacy, often with disappointing results [15,16]. Selecting the most promising substances is therefore important to avoid costly failures [17].

Cellular reduction–oxidation (redox) state is directly affected in conditions of oxidative stress, and depletion of endogenous antioxidants plays a critical role in disease progression [18]. Genetically encoded indicators can be targeted to specific organelles of interest and expressed in a wide variety of cells and organisms [19]. The indicator used in this work, redox-sensitive green fluorescent proteins (roGFP1), allows the real-time visualization of the oxidation state of the indicator [20,21]. In roGFP1 (GFP with mutations C48S, S147C, and Q204C), two surface-exposed cysteines are placed at Positions 147 and 204 on adjacent β-strands close to the chromophore. Disulfide formation between the cysteine residues promotes protonation of the chromophore and increases the excitation spectrum peak near 400 nm at the expense of the peak near 490 nm. The ratios of fluorescence from excitation at 400 and 490 nm indicate the extent of oxidation and thus the redox potential while canceling out the amount of indicator and the absolute optical sensitivity [20,21]. In contrast to its close cousin roGFP2, roGFP1 also offers the advantage to be insensitive to variations in pH [21].

Abbreviations: AX, astaxanthin; CCD, charge-coupled device; DCF, 2′,7′-dichlorofluorescein; DMEM/F12, Dulbecco's modified Eagle medium/F-12 nutrient mixture; DNP, 2,4-dinitrophenol; FBS, fetal bovine serum; GFP, green fluorescent protein; H_2DCFDA, 2′,7′-dichlorodihydrofluorescein diacetate; JC-1, 5,5′,6,6′-tetrachloro-1,1′,3,3′-tetraethylbenzimidazolylcarbocyanine iodide; N.A., numerical aperture; PBS, phosphate buffered saline; roGFP, redox-sensitive green fluorescent protein; TMRM, tetramethyl rhodamine methyl ester.

* Corresponding author. Tel.: +81 44 733 9267; fax: +81 44 733 9268.
E-mail address: ohta@nms.ac.jp (S. Ohta).

0955-2863/$ – see front matter © 2010 Elsevier Inc. All rights reserved.
doi:10.1016/j.jnutbio.2009.01.011

Astaxanthin (AX), a red-orange carotenoid pigment, is a powerful antioxidant that occurs naturally in a wide variety of living organisms and has positive effects on cancer, diabetes, the immune system, and ocular health [22]. Health benefits such as cardiovascular disease prevention, immune system boosting, bioactivity against *Helicobacter pylori*, and cataract prevention have been associated with AX [23]. Oral supplementation of a synthetic AX derivative reduced lipid peroxidation levels and provided significant cardioprotection, consistent with its lipophilic nature and in vitro antioxidant properties [24]. However, the concentrations of AX used in these studies were generally much higher than what can be achieved using supplementation [25] or dietary intervention [26]. We investigated how AX could exert an antioxidant effect in a concentration range chosen close to what can be achieved using supplements and/or diet.

2. Materials and methods

2.1. Cell culture

HeLa human cervical cancer cells were maintained in Dulbecco's modified Eagle medium/F-12 nutrient mixture (DMEM/F12) medium (Invitrogen Japan K.K.) supplemented with 10% fetal bovine serum (FBS). Undifferentiated PC12 rat pheochromocytoma cells were cultured in DMEM supplemented with 10% FBS and 5% heat-inactivated horse serum. Jurkat immortalized T lymphocyte cells were cultivated in RPMI1640 (Invitrogen) containing 10% FBS. All media contained 100 U/ml penicillin and 100 μg/ml streptomycin, and all cell types were maintained at 37°C in a humidified atmosphere of 5% CO_2 and 95% air.

2.2. Transfection

HeLa cells were transfected with the mammalian expression vector pEGFP-N1 (Clontech, Takara Bio, CA) containing roGFP1 (for expression in the cytosol) or roGFP1 with a mitochondrial targeting sequence (pyruvate dehydrogenase E1 subunit leader sequence, for expression in mitochondria) using the Effectene Transfection Reagent (Qiagen Japan) according to the manufacturer's protocol. Stable transfectants were selected using 400 μg/ml Geneticin (Invitrogen) for more than 4 weeks and cloned. Expression of roGFP1 was confirmed by its fluorescence.

2.3. Cell viability

Antimycin A (Sigma) was dissolved to 50 mg/ml in dimethyl sulfoxide (DMSO). The medium was changed to DMEM supplemented with 1.0% FBS overnight, and the PC12 cells were then treated with AX (Sigma) at the indicated concentrations for 6 and 24 h in DMEM supplemented with 1.0% FBS. After AX treatment, 20 μg/ml antimycin A was added (final DMSO concentration: 0.1%) and the cells incubated for 20 h. The number of live/dead cells was counted with a fluorescence microscope (Nikon AZ100, Tokyo) using the LIVE/DEAD cell viability kit for mammalian cells (Invitrogen) and the survival rate expressed as live cells/(live cells+dead cells).

2.4. Fluorescence microscopy

Fluorescence images were recorded using a multidimensional imaging workstation (AS MDW, Leica Microsystems, Wetzlar, Germany) consisting of a tunable light source (Polychrome IV monochromator, Till Photonics, Gräfelfing, Germany), an inverted epifluorescence microscope (DM IRE2, Leica Microsystems) contained in a climate chamber maintained at 37°C and a cooled charge-coupled device (CCD) camera (CoolSnap HQ, Roper Scientific, Princeton, NJ). A 0.35× demagnifiying lens (Leica Microsystems) was inserted between the microscope and the CCD camera. The components were controlled by custom-made software written in C (Bloodshed Dev-C ++) and LabVIEW (National Instruments, Austin, TX).

2.5. Redox-sensitive fluorescent protein fluorescence recording

HeLa cells expressing roGFP1 were washed with PBS and fluorescence recorded. Hydrogen peroxide was diluted from a 30% (w/v) stock solution with phosphate buffered saline (PBS) (37°C) to 500 μM and added to reach the indicated concentration. Dual excitation ratio imaging was performed using a 20× objective [numerical aperture (N.A.) 0.5] and 800 ms exposure time at 410 and 490 nm excitation wavelength. A 500-nm short pass excitation filter (E500SP), 515 nm extended-range dichroic mirror (515DCXR) and 520–600 nm bandpass emission filter (HQ560/80, all from Chroma Technology Corporation, Rockingham, VT) was used for both wavelengths.

Fluorescence data were analyzed using MATLAB (MathWorks, Version 7 Release 14, Natick, MA). After subtracting background fluorescence and CCD dark field, areas corresponding to cells were automatically selected using the criteria of more than 10 connected pixels with fluorescence intensity above both 3% of the maximum fluorescence in the field of view and more than 8 standard deviations above the background noise/intensity in the image obtained with 410 nm excitation wavelength. Such regions were marked and visually confirmed to correspond to cells expressing fluorescent protein. The fluorescence ratio was formed by dividing the fluorescence integral of such regions at 410 and 490 nm excitation. When following the time course of the fluorescence ratio of individual cells, in order to be counted, cells had to fulfill the above criteria at every recorded time point.

2.6. Mitochondrial membrane potential

A 0.5-mM stock solution of 5,5′,6,6′-tetrachloro-1,1′,3,3′-tetraethylbenzimidazolylcarbocyanine iodide (JC-1; Invitrogen) was prepared in equal volumes of ethanol and DMSO. HeLa cells were cultured in DMEM/F12+10% FBS with or without 800 nM AX (control: DMSO) for 6 h, 1 day and 2 days, then stained with 250 nM JC-1 in culture medium for 60 min, washed with PBS and fluorescence recorded immediately, all at 37°C. Dual excitation ratio imaging was performed using a 20× objective (N.A. 0.5) and 200 ms exposure time at 520 nm and 570 nm excitation wavelength. A 580 nm short pass excitation filter (E580SP), 585 nm extended range dichroic mirror (585DCXR) and 590- to 670-nm bandpass emission filter (HQ635/60, all from Chroma Technology Corporation) was used for both excitation wavelengths. Fluorescence data was analyzed using MATLAB (MathWorks, Version 7 Release 14). After subtracting background (dark field) fluorescence, areas corresponding to cells were automatically selected using the criteria of more than 10 connected pixels with fluorescence intensity above both 3% of the maximum fluorescence in the field of view and more than 8 standard deviations above the background noise/intensity in the image obtained with 520 nm excitation wavelength. The fluorescence ratio was formed by dividing the fluorescence integral of all such regions at 570 nm and 520 nm excitation. The field of view usually contained about 100 to 200 cells.

2.7. Superoxide measurement

HeLa cells were cultured in DMEM/F12+10% FBS with or without 800 nM AX (control: DMSO) for 6 h, 1 day and 2 days, then exposed to 30 μg/ml antimycin A for 15 min, then 250 nM MitoSOX Red (Invitrogen) and 500 nM Hoechst34580 (Invitrogen) added and incubated for 60 min, and fluorescence recorded using a 20× (N.A. 0.5) objective. Hoechst34580 fluorescence was excited at 395 nm in combination with a 500-nm short-pass excitation filter (E500SP), 515 nm extended-range dichroic mirror (515DCXR) and 520–600 nm bandpass emission filter (HQ560/80). Ethidium (MitoSOX Red oxidation product) fluorescence was excited at 520 nm and recorded using a 580-nm short-pass excitation filter (E580SP), 585 nm extended range dichroic mirror (585DCXR) and 590–670 nm bandpass emission filter (HQ635/60). Fluorescence data was analyzed using MATLAB (MathWorks, Version 7 Release 14). After subtracting background (dark field) fluorescence, cell nuclei were automatically detected using the criteria of more than 25 connected pixels with fluorescence intensity above both 20% of the maximum fluorescence in the field of view and more than 10 standard deviations above the background noise/intensity in the Hoechst 34580 image. Mean ethidium fluorescence intensity in the area above the nucleus was used as the measure of superoxide production.

2.8. Flow cytometry

Jurkat cells were cultivated in medium in the presence or absence (DMSO) of AX (800 nM) for 6 h, 1 day and 2 days without medium change. There was no difference among the growth rates of these cell cultures. For detection of superoxide anion, cells were incubated with antimycin A (30 μg/ml) for 10 min. Then, MitoSOX Red (250 nM) was added. After 1 h, the cells were analyzed by flow cytometry (Cell Lab Quanta system, Beckman Coulter, Chaska, MN). For detection of hydroxyl peroxides, cells were incubated with 2′,7′-dichlorodihydrofluorescein diacetate (H_2DCFDA) (20 μM, Invitrogen). After 15 min, antimycin A (30 μg/ml) was added. One hour later, the cells were analyzed by flow cytometry as above. Ten thousand cells of normal size (assessed by forward scattering) were analyzed under each condition.

2.9. Physiologically occurring (basal) oxidative stress

Cells were cultured in DMEM/F12+10% FBS with or without 800 nM AX (control: DMSO) for 2 days then incubated with 20 μM H_2DCFDA and 500 nM Hoechst34580 in medium for 60 min, washed with PBS and the dichlorofluorescein (DCF) fluorescence of individual cells measured immediately afterward using a 20× objective (N.A. 0.5). Fluorescence was recorded using the BGR triple bandpass filter set (Leica Microsystems). Hoechst34580 was excited at 403 nm and DCF at 496 nm wavelength. Fluorescence data were analyzed using MATLAB (MathWorks, Version 7 Release 14). After subtracting background (dark-field) fluorescence, cell nuclei were automatically detected using the criteria of more than 25 connected pixels with fluorescence intensity above both 5% of the maximum fluorescence in the field of view and more than 10 standard deviations above the background noise/intensity in the Hoechst 34580 image. Mean DCF fluorescence intensity in the area above the nucleus was used as the measure of oxidative stress.

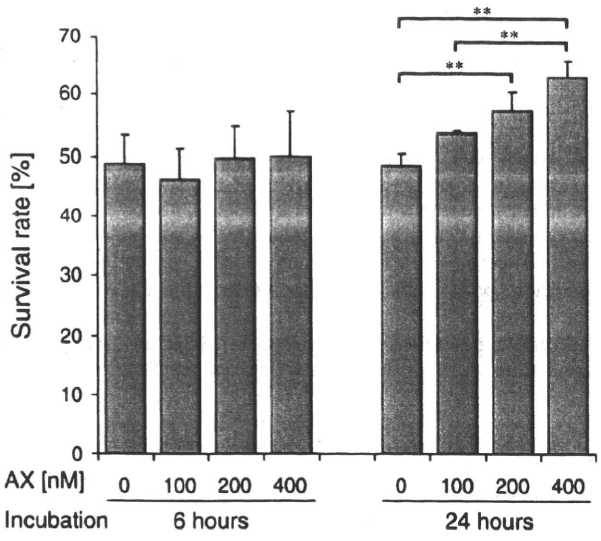

Fig. 1. Astaxanthin effect on PC12 cell survival under oxidative stress. Cells were cultured in the presence of 0, 100, 200 and 400 nM AX for 6 h or 24 h and then exposed to 30 μg/ml antimycin A as described under cell viability in Materials and methods. No effect was detected when cells were preincubated with AX for 6 h. When preincubated with AX for 24 h, cells were protected against cell death induced by oxidative stress, significantly for 200 and 400 nM AX ($P<.01$). Data are means±S.D. from three fields containing 100–200 cells each.

2.10. Oxygen consumption

HeLa cells were cultured in DMEM/F12+10% FBS with or without 800 nM AX (control: DMSO) for 6 h, 1 day and 2 days, trypsinized and resuspended in DMEM/F12. Oxygen consumption was measured using the Oxygen Meter Model 781 and the Mitocell MT200 closed respiratory chamber (Strathkelvin Instruments, North Lanarkshire, UK), continuously stirred at 37°C. The oxygen respiration rate was calculated in the following three conditions: basal rate (no additions), State 4 [after addition of 2 μM oligomycin (Sigma)], uncoupled [after addition of 80 μM 2,4-dinitrophenol (DNP); Sigma] using the Strathkelvin 949 Oxygen System software. Cell concentration was determined using a hemocytometer.

2.11. Confocal microscopy

To confirm targeting of roGFP1 to the mitochondrial matrix, HeLa cells expressing the mitochondrial targeting vector were cultured in a glass-bottom dish and stained with 40 nM tetramethyl rhodamine methyl ester (TMRM, Molecular Probes, Invitrogen) for 20 min. Fluorescence was observed using a FluoView FV300 confocal microscope (Olympus, Tokyo, Japan) with a 60× (N.A. 1.4) oil immersion objective. roGFP1 was excited at 488 nm and emission collected above 510 nm, while TMRM was excited at 543 nm and emission collected above 570 nm.

2.12. Statistical calculations

Statistical significance was determined using the unpaired two-tailed Student's t test in Excel (Microsoft, Redmond, WA) or one-way analysis of variance (ANOVA) followed by a Tukey–Kramer multiple comparison test in Matlab (MathWorks, Version 7 Release 14). Error bars indicate the standard deviation of three or more measurements. The number of asterisks indicates statistical significance. Specifically, * indicates $P<.05$, ** indicates $P<.01$ and *** indicates $P<.001$.

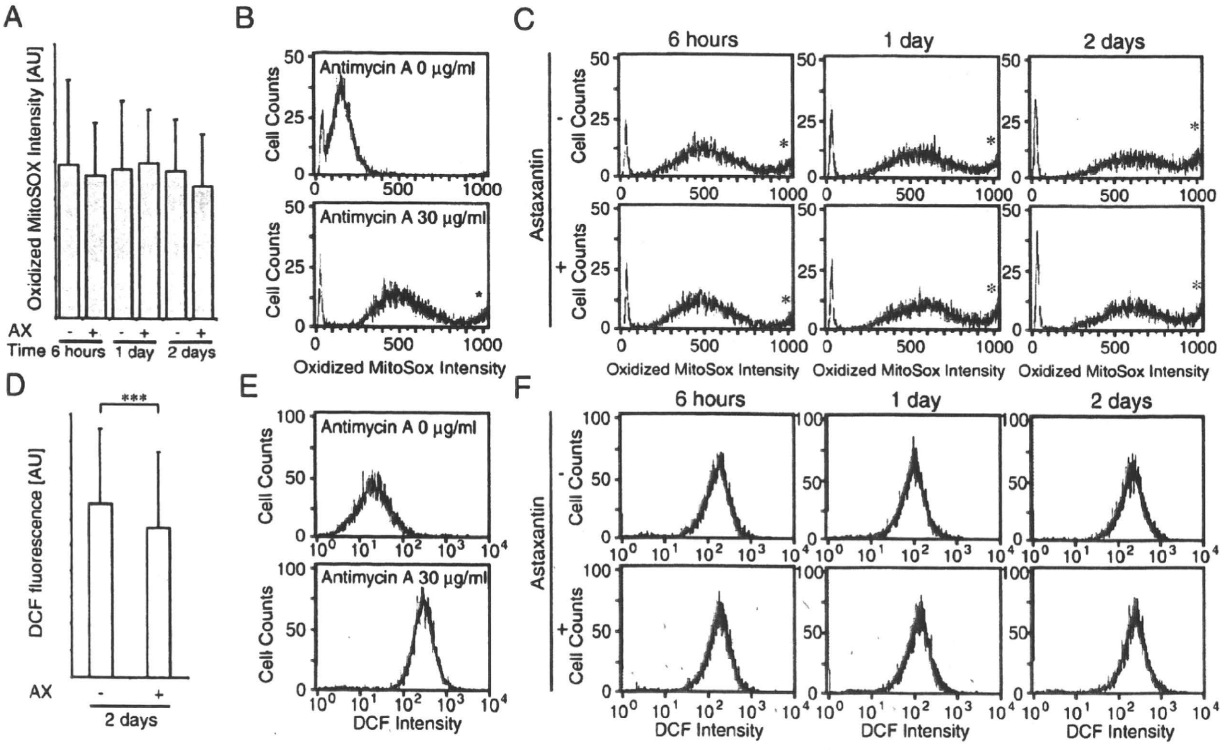

Fig. 2. Superoxide and oxidative stress. (A) PC12 cells were preincubated with AX for indicated periods, followed by exposure to antimycin A to induce superoxide. Superoxide, as measured using MitoSOX Red, was not changed significantly by culturing cells with AX. Data were obtained as the means±S.D. by quantifying signal intensities of 70–100 cells. (B) Superoxide production is induced by incubating Jurkat cells with 30 μg/ml antimycin A. (C) Jurkat cells cultivated in the presence or absence (DMSO) of AX (800 nM) for 6 h, 1 day, and 2 days were treated with antimycin A (30 μg/ml). No significant difference in the amount of oxidized MitoSOX Red was observed, indicating that, under conditions of oxidative stress and at a concentration of 800 nM, AX is unable to scavenge significant amounts of superoxide. (D) Basal oxidative stress level in cells, as measured by incubating cells with H_2DCFDA. AX significantly decreased the amount of DCF produced in HeLa cells incubated with AX for 2 days ($n=383$ cells, control: $n=403$ cells; from three independent experiments under each condition). *** $P<.001$. (E) Antimycin A (30 μg/ml) also induced acute oxidative stress as assessed using H_2DCFDA. The amount of DCF produced was increased more than 10-fold. (F) Similar to C, AX did not reduce acute oxidative stress. No significant difference in the amount of DCF was observed.

3. Results

3.1. AX improves cell survival under oxidative stress

To test whether AX protects cells against oxidative stress, we exposed rat adrenal pheochromocytoma (PC12) cells, a neuronal model cell line shown to be sensitive to oxidative stress [27], to antimycin A. Antimycin A, an inhibitor of complex III of the electron transport chain, induces oxidative stress by increasing mitochondrial superoxide production [28] (see also Fig. 2B and E). Preincubation with AX for 6 h did not significantly increase PC12 cell survival, but when cells were exposed to AX for 24 h, a significant increase in the number of surviving cells was observe with more than 200 nM AX, demonstrating that AX was able to protect PC12 cells against oxidative stress at relatively low concentrations (Fig. 1). The effect was concentration dependent, with 400 nM AX being more protective than 100 nM AX ($P<.01$).

3.2. AX reduces basal oxidative stress levels but not acute oxidative stress

To determine the mechanism by which AX protects against oxidative stress, we determined whether AX was able to directly scavenge superoxide radical. Human cervical cancer (HeLa) and T lymphocyte (Jurkat) cells were exposed to antimycin A as an acute stress model, and oxidation of the superoxide-sensitive probe MitoSOX Red quantified as described in Materials and methods. Preincubation of cells with 800 nM AX did not significantly reduce the

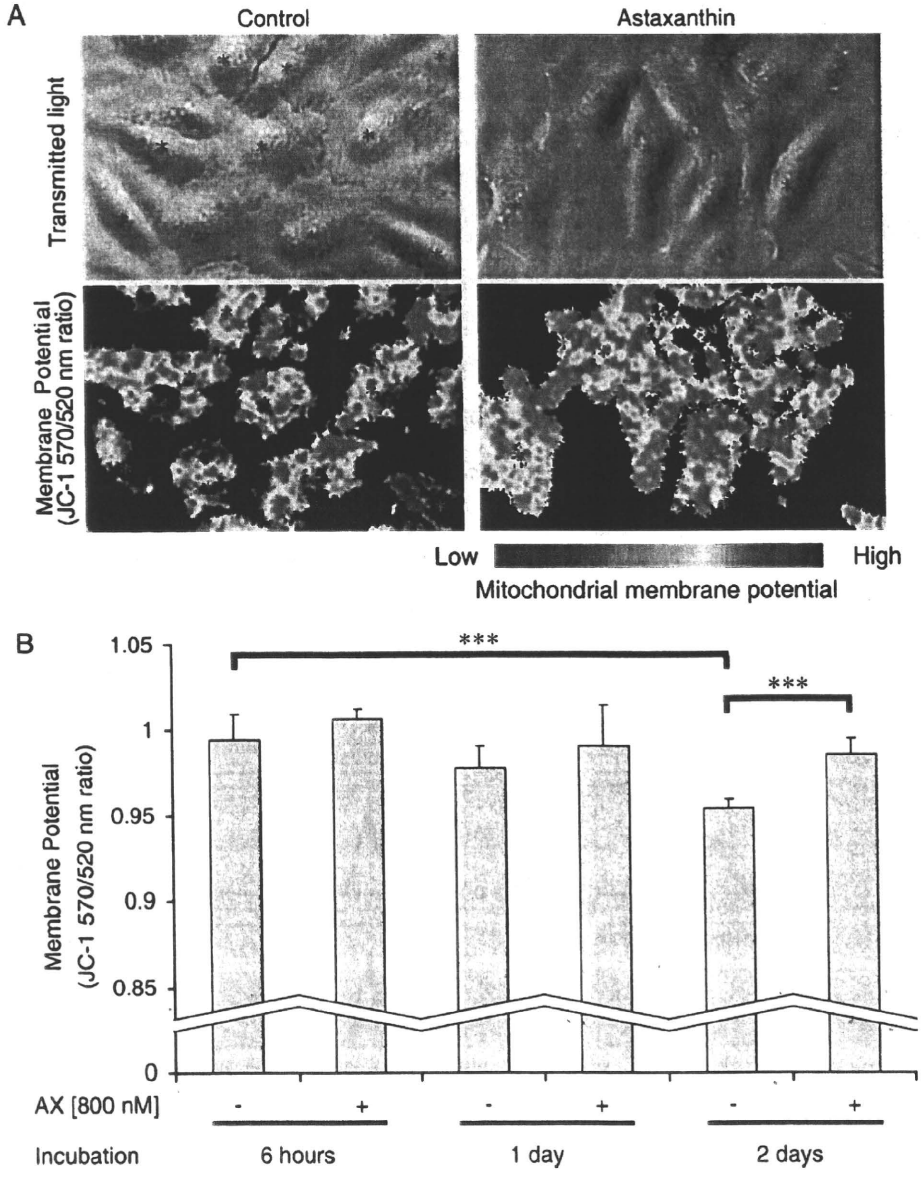

Fig. 3. Mitochondrial membrane potential. (A) Representative transmitted light (upper row) and membrane potential (lower row) images of HeLa cells cultured for 2 days in the presence (right) or absence (left) of 800 nM AX. The membrane potential image was created by color coding the dual excitation fluorescence ratio. Asterisks (pink) mark the approximate positions of cell nuclei. (B) Average JC-1 dual excitation fluorescence ratio from three independent experiments, with fluorescence recorded at 2 locations for each experiment. Membrane potential was significantly higher ($P<.001$) in the presence of AX after 2 days in culture, but rather than increasing the mitochondrial membrane potential, AX seemed to prevent a loss of membrane potential that occurred with increasing time in culture.

amount of superoxide detected (Fig. 2A), suggesting that AX did not scavenge excess amounts of superoxide under this unphysiological condition. Similarly, Jurkat cells were treated with antimycin A-generated superoxide anion (as assessed by MitoSOX Red) and reactive peroxides (as assessed by H_2DCFDA) to a great extent (Fig. 2B and E). In these flow cytometry experiments, the population of cells with an intensity of 1000 or more (marked with * in Fig. 2B and C) was between 2% and 4% of the cells analyzed. Quantitative analysis revealed no significant difference in the fluorescence intensity of oxidized MitoSOX product (Fig. 2C) or DCF (Fig. 2F) between AX-treated or nontreated cells, even when cells were treated with AX for 2 days. Post-addition of AX did not change fluorescent patterns of the antimycin A-treated cells without AX treatment (data not shown), indicating that AX does not interfere with fluorescence of oxidized MitoSOX and DCF.

However, when the basal level of oxidative stress, that is the physiologically occurring oxidative stress, in HeLa cells was determined using the oxidant sensitive probe 2′,7′-dichlorodihydrofluorescein, AX significantly reduced the amount of fluorescent oxidation product (DCF) produced (Fig. 2D), indicating that AX is able to reduce endogenous oxidative stress. This signifies that there is a low but detectable amount of endogenous oxidative stress under normal culture conditions, which AX can reduce.

3.3. AX helps maintain the mitochondrial membrane potential

We proceeded to determine whether such endogenous oxidants affect cellular function and whether AX could influence it. The mitochondrial membrane potential was quantified using the aggregate-forming probe JC-1 [29]. Using dual excitation ratio imaging, we observed a significantly higher mitochondrial membrane potential when AX was present in culture after 2 days (Fig. 3A). For shorter incubation times, the difference was not significant. Interestingly, rather than increasing the mitochondrial membrane potential, AX seemed to slow down a gradual loss of membrane potential that may occur with time in culture. While a significant loss in the membrane potential occurred from 6 h to 2 days in culture without AX (Fig. 3B, $P<.001$), no significant difference/loss could be detected in the presence of AX.

3.4. AX effect on respiratory control

Speculating that a decrease in mitochondrial membrane could also affect mitochondrial respiration, we measured the oxygen consumption of intact HeLa cells cultured under the same conditions. Measuring first baseline oxygen consumption (no additions), then the mitochondrial State 4 consumption (by blocking complex V with oligomycin) and then maximal oxygen consumption by uncoupling mitochondria with DNP (80 μM) (Fig. 4A), we could not observe significant changes in the absolute consumption rates (Fig. 4B), but the ratio of baseline to uncoupled oxygen consumption was significantly higher in the presence of AX, that is, mitochondria were more active in the presence of AX (Fig. 4C). In addition, the relative reduction in oxygen consumption upon addition of oligomycin was increased in the presence of AX (Fig. 4C). Together, these findings suggest that AX stimulates respiration probably by maintaining a higher membrane potential (Fig. 3).

3.5. AX improves the mitochondrial redox state

Due to these positive but rather subtle effects of AX on mitochondrial function, we looked for a sensitive method to detect relatively mild oxidative stress at the organelle level. We chose redox-sensitive GFP as a promising method since it is ratiometric and can be targeted to various cellular compartments [20,21,30]. Furthermore, it has been shown to be a quantitative sensor for the redox potential of the cellular glutathione redox buffer [31]. HeLa

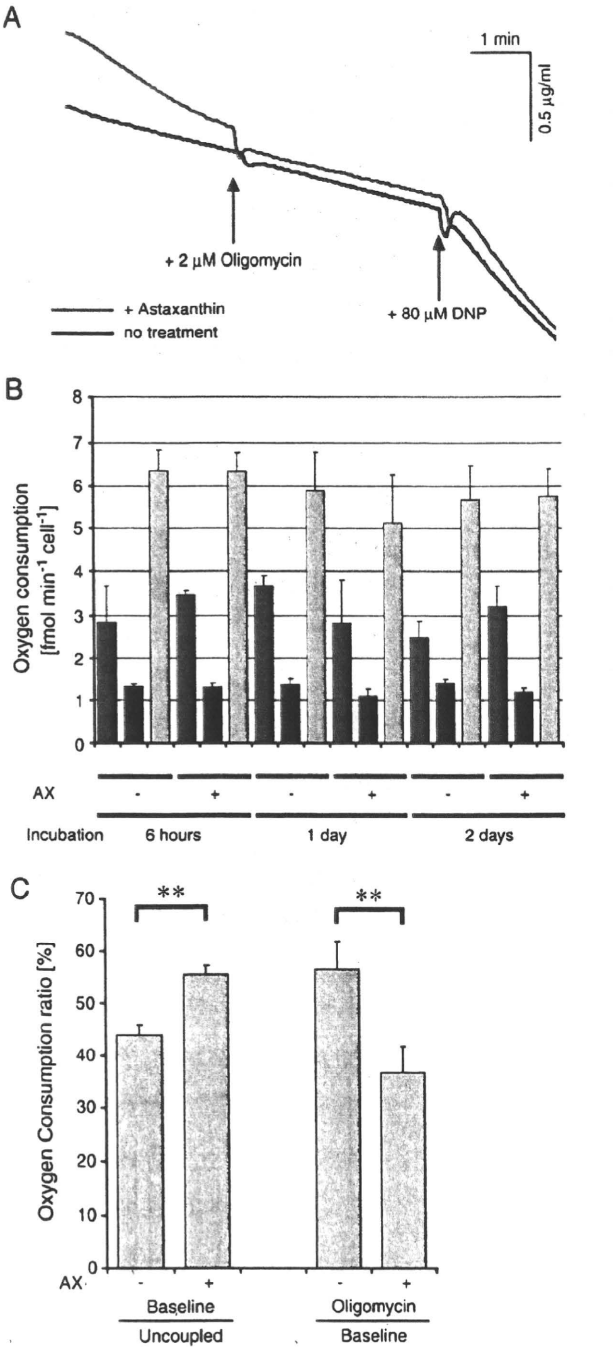

Fig. 4. Oxygen consumption profiles. (A) Representative traces of the oxygen consumption of intact HeLa cells cultured with (800 nM, red trace) or without (black trace) AX. Oligomycin and DNP were added at the indicated (arrows) time points. (B) Average oxygen consumption per cell under baseline conditions (BL; dark gray bars), in the presence of 2 μM oligomycin (+OM; black bars) and when uncoupled with 80 μM DNP (+DNP, light gray bars). Data are the average±S.D. of three measurements of cells cultured for 6 h (6H), 1 day (1D) or 2 days (2D) in the presence or absence of 800 nM AX (control: DMSO). (C) AX increased the ratio of baseline divided by uncoupled oxygen consumption and decreased the ratio of oxygen consumption in the presence of oligomycin divided by baseline oxygen consumption. Data are mean±S.D. ** $P<.01$.

cells were stably tranfected with the expression vector for roGFP1 targeted to mitochondria as described above and the colocalization of roGFP1 with mitochondria confirmed using confocal microscopy. RoGFP1 showed almost perfect overlap with the mitochondrial marker dye TMRM (Fig. 5A). Cells expressing mitochondrial roGFP1 showed no abnormal morphology (Fig. 5A and B), and mitochondria exhibited the characteristic tubular shape and movement presumably along microtubules (Supplementary Movie). The mitochondrial redox state of individual cells was measured using dual excitation imaging (Fig. 5C). Mitochondrial roGFP1 (basal redox state) was more reduced in cells cultured with AX for 6 h, 1 day and 2 days (Fig. 5D and E). Mitochondrial ability to maintain the reducing

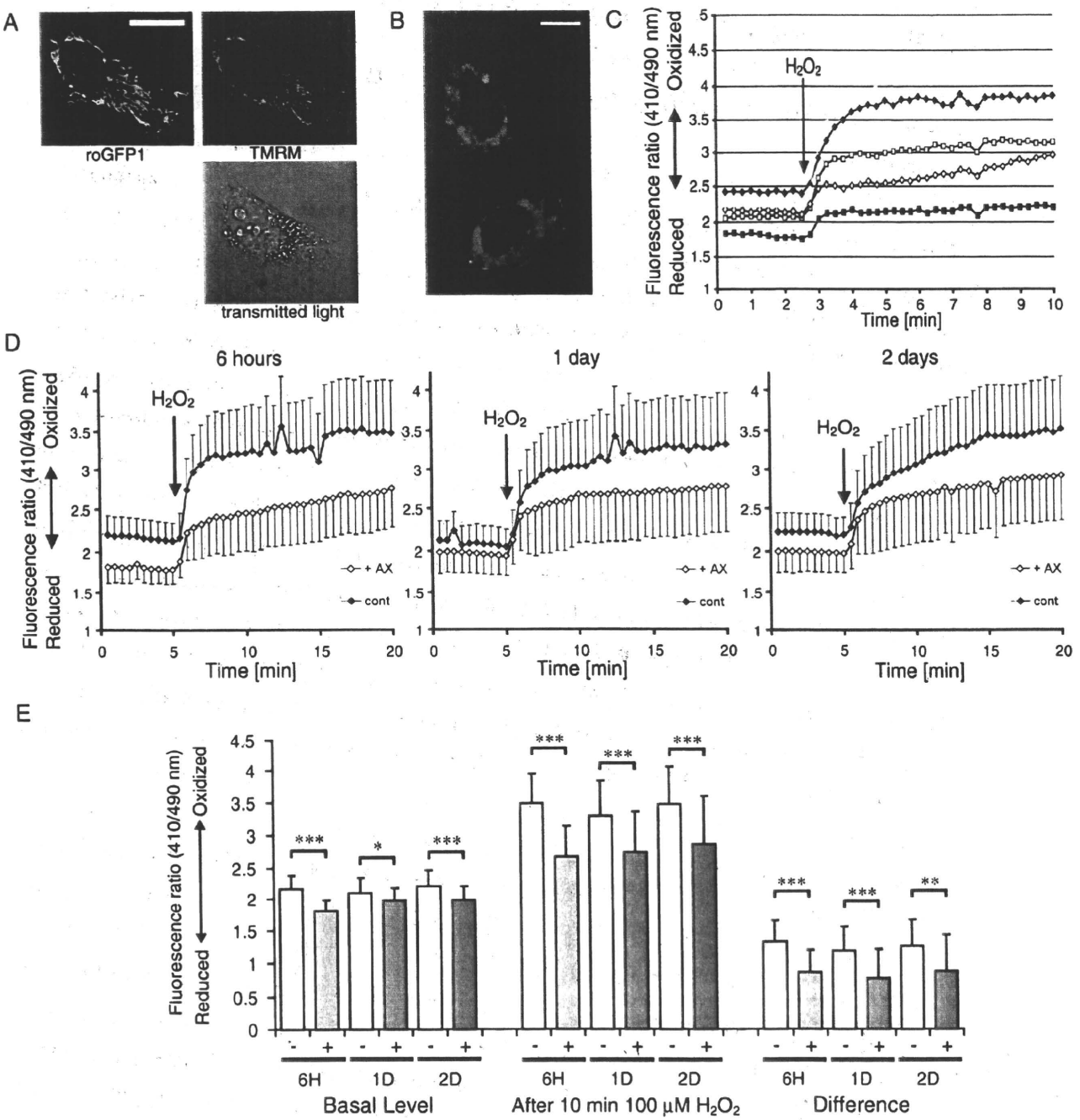

Fig. 5. Mitochondrial redox state measured using redox-sensitive GFP. (A) Confocal and transmitted light images of a HeLa cell expressing roGFP1 targeted to mitochondria. Overlap of TMRM and roGFP1 fluorescence confirms mitochondrial localization of roGFP1. Scale bar: 20 µm. (B) Epifluorescence image of HeLa cells expressing roGFP1 targeted to mitochondria. Regions automatically selected for analysis are marked in pink. Scale bar: 20 µm. (C) Representative traces of the roGFP1 redox state time course (dual excitation fluorescence ratio). Four individual cells show the heterogeneity of mitochondrial redox state between cells. After the indicated periods, 100 µM hydrogen peroxide was added (arrow). (D) Average time course indicating mitochondrial redox state of cells cultured with or without 800 nM AX for 6 h (6H) (+AX: $n=35$ cells, control: $n=34$ cells), 1 day (1D) (+AX: $n=41$ cells, control: $n=32$ cells) or 2 days (2D) (+AX: $n=32$ cells, control: $n=27$ cells). Average baseline as well as redox state after addition of 100 µM hydrogen peroxide (arrow) was more reduced when AX was present. (E) Average baseline fluorescence ratio, ratio after addition of hydrogen peroxide and amount of oxidation (ratio difference) induced by hydrogen peroxide were significantly lower, that is, reduced when AX was present. Data are mean±S.D. $^{*}P<.05$, $^{**}P<.01$, $^{***}P<.001$.

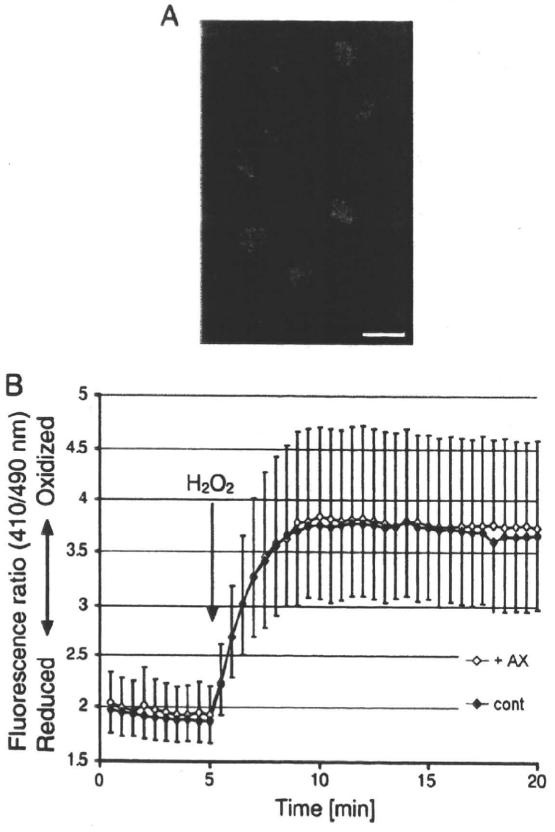

Fig. 6. Effect of AX on the cytosol redox state. (A) Epifluorescence image of HeLa cells expressing roGFP1 in the cytosol. Regions automatically selected for analysis as individual cells are marked in pink. Scale: 20 μm. (B) Time course of cytosol redox state (410/490 nm dual excitation fluorescence ratio) upon addition of 100 μM H_2O_2 (arrow). No difference was detected, neither in the basal redox state nor in the change or state after addition of H_2O_2, between cells cultured for 2 days in the presence (open diamonds, n=73 cells) or absence (filled diamonds, n=90 cells) of 800 nM AX.

environment was then tested by exposing cells to 100 μM H_2O_2, which quickly oxidized mitochondrial roGFP1 but significantly less so when AX was present (Fig. 5D and E). To exclude the possibility that the more reduced state after addition of H_2O_2 is simply a consequence of the more reduced (basal) state prior to addition of H_2O_2, we also compared the change in fluorescence ratio induced by H_2O_2. This difference was also significantly smaller in the presence of AX (Fig. 5E). Whether this antioxidant effect of AX was limited to mitochondria or also extended to the cytosol was tested using cells expressing roGFP1 in the cytosol (Fig. 6A). The basal redox state and resistance to oxidative challenge with H_2O_2 were tested in the same manner as for mitochondria, but no effect of AX on the redox state of the cytosol could be detected (Fig. 6B).

4. Discussion

The results above demonstrate that, under basal conditions, AX had a small but significant positive effect on mitochondrial function (higher membrane potential, higher respiratory control). This is reassuring since endogenous oxidative stress, though clearly present [32], should be rather mild in the absence of external stress-inducing agents. Since mitochondria are a major source of reactive oxygen species (ROS) in the cell, accumulation of AX in the mitochondrial membrane would potentiate its antioxidant effects. There is a report showing AX protects mesangial cells from hyperglycemia-induced oxidative signaling [33]. The fact that AX was able to maintain mitochondria but not the cytosol in a reduced state (Fig. 5) indicates that the effect of AX is, at least during mild, endogenous oxidative stress, concentrated on mitochondria. The effect of AX became more pronounced with incubation time. Interestingly, such a time dependency was also observed in an investigation of the antitumor activity of AX [34]. AX, at a total serum concentration of approximately 1.2 μM, suppressed tumor cell growth when mice were fed AX before inoculation but was ineffective when the AX-supplemented diet was started at the same time as tumor inoculation [34].

Cell types differ in their dependence on mitochondria-generated ATP as a source of energy and in their sensitivity to oxidative stress. AX protected PC12 cells against antimycin A-induced cell death. HeLa cells, in contrast, can rely on glycolysis as the sole energy supply and survive even in the absence of a functional electron transport chain [35]. Accordingly, blocking electron transport with antimycin A, though clearly inducing oxidative stress, does not necessarily lead to HeLa cell death [36,37]. That AX was protective in both cells lines indicates that the effect of AX should not be cell type or cancer specific [38]. Moreover, mitochondria isolated from PC12 cells had oxygen consumption rates similar to isolated rat liver mitochondria (data not shown) [39], indicating that the effects of AX described here are not specific to those of cancer-type cells.

Although direct superoxide scavenging by a highly water-dispersible carotenoid phospholipid has been reported at high concentrations [40], AX may not exert its strong effect by scavenging superoxide. In fact, under conditions of acute oxidative stress when large amounts of ROS are produced, AX showed no detectable effect, indicating that the effects of AX are not due direct scavenging of ROS such as superoxide or peroxides (Fig. 2A). This is to be expected since superoxide is a charged radical unable to cross cellular membranes and carotenoids are extremely lipophilic. On the other hand, since AX reduced the endogenous oxidative stress level (Fig. 2D), it is reasonable to assume it protects cells against oxidative damage in the lipid phase (Fig. 1). Thus, even though it may not scavenge ROS directly, AX has the potential to protect cells against damage mediated by oxidative stress. Since ROS including superoxide and hydrogen peroxide play significant roles in the signal transduction at low concentrations [41], this characteristic of AX suggests little possibilities of negative side effects of AX consumption.

The increase in mitochondrial oxygen consumption of AX-treated cells is probably in part a consequence of the change in mitochondrial membrane potential [41]. The relatively higher reduction in oxygen consumption upon addition of oligomycin in the presence of AX would be expected as mitochondrial membrane potential is higher in the presence of AX, while in the absence of AX, oligomycin is unable to increase membrane potential to the same level. Such an inhibition of respiration upon inactivation of complex V is referred to as "respiratory control ratio," an important measure of mitochondrial health when investigating isolated mitochondria [41], even though it should be pointed out that we used intact cells, where respiration during stimulation of complex V with ADP is not accessible, and the ratios are not comparable. Physiological effects of AX have been shown to include stimulation of β-oxidation for fatty acids [42,43]. This would be of considerable benefit in reducing obesity and metabolic syndrome in affluent societies. Much of the benefit of one of the most effective drugs for diabetes, metformin, has been attributed to activation of AMP-dependent kinase, which helps by reducing gluconeogenesis and driving oxidation of fat in muscle mitochondria [44]. The AX concentration upon which a significant benefit could be observed (200 nM, Fig. 1) is also well within the range that can be achieved with supplementation. A single oral dose of 10 mg AX resulted in a peak plasma concentration of ~130 nM, whereas a single dose of 100 mg AX resulted in a peak plasma concentration of ~470 nM, with half-lives in the order of days [25]. Similarly, daily consumption of 250 g of either wild or farmed salmon

(farmed salmon is fed synthetic AX to give it its natural coloring) lead to a plateau of ~50 nM AX in plasma after about 6 days [26].

Redox-sensitive GFP targeted to mitochondria could detect changes in the mitochondrial redox state even after short incubation with AX, where conventional methods failed. This indicates that roGFP is a powerful tool for measuring oxidative stress and redox balance at the organelle level. Targeting roGFP to mitochondria allowed us to detect changes in the mitochondrial redox state that were too small to affect the cytosol. Redox-sensitive GFP possibly interacts with a number of cellular enzymes and redox couples, but it is still unclear which determine the roGFP1 redox state to what extent. The reduction of roGFP1 is likely enzyme-dependent, as reductase and dehydrogenase inhibitors reduced or prevented reduction of the close cousin roGFP2 in the cytosol [20]. Conversely, oxidation of roGFP proceeded considerably faster when, compared to the isolated protein, it was expressed in cells, suggesting that the oxidation is also catalyzed by intracellular enzymes. In our hands, the response of roGFP1 to hydrogen peroxide was also significantly faster than previously reported [20]. RoGFP oxidation was observed immediately, and the maximum response in the cytosol was reached within 5 min (Fig. 6B).

The high sensitivity of roGFP to changes in organelle redox state suggests that it is a powerful tool to investigate the biochemistry of oxidative stress and redox balance at the organelle level. Accurate measurement of oxidative stress is an ongoing challenge, and despite the availability and ongoing development of a wide range of probes and methods, their correct use is often complicated (e.g., Ref. [45]) and/or cumbersome (e.g., Ref. [46]). The most widely employed method to "quantify" ROS, the conversion of dichlorodihydrofluorescein (H_2DCF) to DCF, requires a catalyst for H_2DCF to be oxidized by hydrogen peroxide and reacts indiscriminately with a variety of oxidizing factors, including light and itself [47,48].

RoGFP1 is a relatively new nondestructive and ratiometric sensor for cellular redox state [20,21] permitting a wide range of measurements previously impossible or extremely labor-intensive and therefore open to errors and artefacts. Experiments to establish the sensitivity of roGFP1 to various stressors and antioxidants are currently under way in our laboratory, but in our opinion, roGFP offers great promise for pin-point detection of oxidative stress. Targeting roGFP1 to subcellular structures allowed us to observe oxidative stress restricted to mitochondria without affecting the cytosol, demonstrating that changes in redox state and oxidative stress can be confined to cellular compartments. To understand cellular redox states, it might therefore be important to determine compartmental redox states independently. Furthermore, transgenic animals expressing roGFPs should be a valuable tool to test the efficacy of treatments aimed at reducing oxidative stress.

Acknowledgments

We express our deep gratitude to Prof. Jim Remington and his team for kindly providing the roGFP1 containing plasmids. Alexander Wolf was supported by a Postdoctoral Fellowship and grant from the Japan Society for the Promotion of Science.

Appendix A. Supplementary data

Supplementary data associated with this article can be found, in the online version, at doi:10.1016/j.jnutbio.2009.01.011.

References

[1] Lusis AJ. Atherosclerosis. Nature 2000;407:233–41.
[2] Schriner SE, Linford NJ, Martin GM, Treuting P, Ogburn CE, Emond M, et al. Extension of murine life span by overexpression of catalase targeted to mitochondria. Science 2005;308:1909–11.
[3] Serrano M, Blasco MA. Cancer and ageing: convergent and divergent mechanisms. Nat Rev Mol Cell Biol 2007;8:715–22.
[4] Houstis N, Rosen ED, Lander ES. Reactive oxygen species have a causal role in multiple forms of insulin resistance. Nature 2006;440:944–8.
[5] Brownlee M. Biochemistry and molecular cell biology of diabetic complications. Nature 2001;414:813–20.
[6] Beal MF. Bioenergetic approaches for neuroprotection in Parkinson's disease. Ann Neurol) 2003;53(Suppl 3):S39–47 [discussion S47–38].
[7] Dawson TM, Dawson VL. Molecular pathways of neurodegeneration in Parkinson's disease. Science 2003;302:819–22.
[8] Esposito E, Rotilio D, Di Matteo V, Di Giulio C, Cacchio M, Algeri S. A review of specific dietary antioxidants and the effects on biochemical mechanisms related to neurodegenerative processes. Neurobiol Aging 2002;23:719–35.
[9] Finkel T. Radical medicine: treating ageing to cure disease. Nat Rev Mol Cell Biol 2005;6:971–6.
[10] Kim MS, Park JY, Namkoong C, Jang PG, Ryu JW, Song HS, et al. Anti-obesity effects of alpha-lipoic acid mediated by suppression of hypothalamic AMP-activated protein kinase. Nat Med 2004;10:727–33.
[11] Klaus S, Pultz S, Thone-Reineke C, Wolfram S. Epigallocatechin gallate attenuates diet-induced obesity in mice by decreasing energy absorption and increasing fat oxidation. Int J Obes (Lond) 2005;29:615–23.
[12] Borra MT, Smith BC, Denu JM. Mechanism of human SIRT1 activation by resveratrol. J Biol Chem 2005;280:17187–95.
[13] Ridinger MH. Nutraceuticals: miracle or meme? Clin Pharmacol Ther 2007;82: 352–6.
[14] Kamel NS, Gammack J, Cepeda O, Flaherty JH. Antioxidants and hormones as antiaging therapies: high hopes, disappointing results. Cleve Clin J Med 2006;73:1049–56, 1058.
[15] Hansen JM, Go YM, Jones DP. Nuclear and mitochondrial compartmentation of oxidative stress and redox signaling. Annu Rev Pharmacol Toxicol 2006;46: 215–34.
[16] Thomson MJ, Puntmann V, Kaski JC. Atherosclerosis and oxidant stress: the end of the road for antioxidant vitamin treatment? Cardiovasc Drugs Ther 2007;21: 195–210.
[17] Vickers AJ. Which botanicals or other unconventional anticancer agents should we take to clinical trial? J Soc Integr Oncol 2007;5:125–9.
[18] Chinta SJ, Andersen JK. Reversible inhibition of mitochondrial complex I activity following chronic dopaminergic glutathione depletion in vitro: implications for Parkinson's disease. Free Radic Biol Med 2006;41:1442–8.
[19] Miyawaki A, Nagai T, Mizuno H. Engineering fluorescent proteins. Adv Biochem Eng Biotechnol 2005;95:1–15.
[20] Dooley CT, Dore TM, Hanson GT, Jackson WC, Remington SJ, Tsien RY. Imaging dynamic redox changes in mammalian cells with green fluorescent protein indicators. J Biol Chem 2004;279:22284–93.
[21] Hanson GT, Aggeler R, Oglesbee D, Cannon M, Capaldi RA, Tsien RY, et al. Investigating mitochondrial redox potential with redox-sensitive green fluorescent protein indicators. J Biol Chem 2004;279:13044–53.
[22] Hussein G, Sankawa U, Goto H, Matsumoto K, Watanabe H. Astaxanthin, a carotenoid with potential in human health and nutrition. J Nat Prod 2006;69:443–9.
[23] Higuera-Ciapara I, Felix-Valenzuela L, Goycoolea FM. Astaxanthin: a review of its chemistry and applications. Crit Rev Food Sci Nutr 2006;46:185–96.
[24] Gross GJ, Hazen SL, Lockwood SF. Seven day oral supplementation with Cardax (disodium disuccinate astaxanthin) provides significant cardioprotection and reduces oxidative stress in rats. Mol Cell Biochem 2006;283:23–30.
[25] Coral-Hinostroza GN, Ytrestoyl T, Ruyter B, Bjerkeng B. Plasma appearance of unesterified astaxanthin geometrical E/Z and optical R/S isomers in men given single doses of a mixture of optical 3 and 3'R/S isomers of astaxanthin fatty acyl diesters. Comp Biochem Physiol C Toxicol Pharmacol 2004;139:99–110.
[26] Rufer CE, Moeseneder J, Briviba K, Rechkemmer G, Bub A. Bioavailability of astaxanthin stereoisomers from wild (*Oncorhynchus* spp.) and aquacultured (*Salmo salar*) salmon in healthy men: a randomised, double-blind study. Br J Nutr 2007:1–7.
[27] Jha N, Jurma O, Lalli G, Liu Y, Pettus EH, Greenamyre JT, et al. Glutathione depletion in PC12 results in selective inhibition of mitochondrial complex I activity. Implications for Parkinson's disease. J Biol Chem 2000;275:26096–101.
[28] Ohsawa I, Ishikawa M, Takahashi K, Watanabe M, Nishimaki K, Yamagata K, et al. Hydrogen acts as a therapeutic antioxidant by selectively reducing cytotoxic oxygen radicals. Nat Med 2007;13:688–94.
[29] Reers M, Smith TW, Chen LB. J-aggregate formation of a carbocyanine as a quantitative fluorescent indicator of membrane potential. Biochemistry 1991;30: 4480–6.
[30] Schwarzer C, Illek B, Suh JH, Remington SJ, Fischer H, Machen TE. Organelle redox of CF and CFTR-corrected airway epithelia. Free Radic Biol Med 2007;43: 300–16.
[31] Meyer AJ, Brach T, Marty L, Kreye S, Rouhier N, Jacquot JP, et al. Redox-sensitive GFP in *Arabidopsis thaliana* is a quantitative biosensor for the redox potential of the cellular glutathione redox buffer. Plant J 2007;52:973–86.
[32] Choksi KB, Nuss JE, Boylston WH, Rabek JP, Papaconstantinou J. Age-related increases in oxidatively damaged proteins of mouse kidney mitochondrial electron transport chain complexes. Free Radic Biol Med 2007;43:1423–38.
[33] Manabe E, Handa O, Naito Y, Mizushima K, Akagiri S, Adachi S, et al. Astaxanthin protects mesangial cells from hyperglycemia-induced oxidative signaling. J Cell Biochem 2007.
[34] Jyonouchi H, Sun S, Iijima K, Gross MD. Antitumor activity of astaxanthin and its mode of action. Nutr Cancer 2000;36:59–65.

[35] Hayashi J, Ohta S, Kikuchi A, Takemitsu M, Goto Y, Nonaka I. Introduction of disease-related mitochondrial DNA deletions into HeLa cells lacking mitochondrial DNA results in mitochondrial dysfunction. Proc Natl Acad Sci U S A 1991;88:10614–8.
[36] Lyamzaev KG, Izyumov DS, Avetisyan AV, Yang F, Pletjushkina OY, Chernyak BV. Inhibition of mitochondrial bioenergetics: the effects on structure of mitochondria in the cell and on apoptosis. Acta Biochim Pol 2004;51:553–62.
[37] Han YH, Kim SH, Kim SZ, Park WH. Antimycin A as a mitochondria damage agent induces an S phase arrest of the cell cycle in HeLa cells. Life Sci 2008;83:346–55.
[38] Yamamoto N, Sawada H, Izumi Y, Kume T, Katsuki H, Shimohama S, et al. Proteasome inhibition induces glutathione synthesis and protects cells from oxidative stress: relevance to Parkinson disease. J Biol Chem 2007;282:4364–72.
[39] Schwerzmann K, Cruz-Orive LM, Eggman R, Sanger A, Weibel ER. Molecular architecture of the inner membrane of mitochondria from rat liver: a combined biochemical and stereological study. J Cell Biol 1986;102:97–103.
[40] Foss BJ, Sliwka HR, Partali V, Cardounel AJ, Zweier JL, Lockwood SF. Direct superoxide anion scavenging by a highly water-dispersible carotenoid phospholipid evaluated by electron paramagnetic resonance (EPR) spectroscopy. Bioorg Med Chem Lett 2004;14:2807–12.
[41] Ainscow EK, Brand MD. Internal regulation of ATP turnover, glycolysis and oxidative phosphorylation in rat hepatocytes. Eur J Biochem 1999;266:737–49.
[42] Aoi W, Naito Y, Takanami Y, Ishii T, Kawai Y, Akagiri S, et al. Astaxanthin improves muscle lipid metabolism in exercise via inhibitory effect of oxidative CPT I modification. Biochem Biophys Res Commun 2008;366:892–7.
[43] Ikeuchi M, Koyama T, Takahashi J, Yazawa K. Effects of astaxanthin in obese mice fed a high-fat diet. Biosci Biotechnol Biochem 2007;71:893–9.
[44] Zhou G, Myers R, Li Y, Chen Y, Shen X, Fenyk-Melody J, et al. Role of AMP-activated protein kinase in mechanism of metformin action. J Clin Invest 2001;108:1167–74.
[45] Johnson-Cadwell LI, Jekabsons MB, Wang A, Polster BM, Nicholls DG. 'Mild Uncoupling' does not decrease mitochondrial superoxide levels in cultured cerebellar granule neurons but decreases spare respiratory capacity and increases toxicity to glutamate and oxidative stress. J Neurochem 2007;101:1619–31.
[46] Arneson KO, Roberts Jr LJ. Measurement of products of docosahexaenoic acid peroxidation, neuroprostanes, and neurofurans. Methods Enzymol 2007;433:127–43.
[47] Wrona M, Wardman P. Properties of the radical intermediate obtained on oxidation of 2′,7′-dichlorodihydrofluorescein, a probe for oxidative stress. Free Radic Biol Med 2006;41:657–67.
[48] Wrona M, Patel KB, Wardman P. The roles of thiol-derived radicals in the use of 2′,7′-dichlorodihydrofluorescein as a probe for oxidative stress. Free Radic Biol Med 2008;44:56–62.